

ABSTRACT

Document Title: AN INTEGRATED METHODOLOGY FOR ASSESSING
FIRE SIMULATION CODE UNCERTAINTY

Victor L. Ontiveros, Master of Science, 2010

Directed by: James Milke, Professor, Department of Fire Protection
Engineering

Fire simulation codes are powerful tools for use in risk-informed and performance-based approaches for risk assessment. Given increasing use of fire simulation code results, accounting for the uncertainty inherent in fire simulation codes is becoming more important than ever. This research presents a “white-box” methodology with the goal of accounting for uncertainties resulting from simulation code. Uncertainties associated with the input variables used in the codes as well as the uncertainties associated with the sub-models and correlations used inside the simulation code are accounted for. A Bayesian estimation approach is used to integrate all evidence available and arrive at an estimate of the uncertainties associated with a parameter of interest being estimated by the simulation code. Two example applications of this methodology are presented.

AN INTEGRATED METHODOLOGY FOR
ASSESSING FIRE SIMULATION CODE UNCERTAINTY

By

Victor L. Ontiveros

Thesis submitted to the Faculty of the Graduate School of the
University of Maryland, College Park, in partial fulfillment
of the requirements for the degree of
Master of Science

2010

Advisory Committee:

Professor James A. Milke, Chair

Professor Mohammad Modarres

Associate Professor Emeritus Frederick W. Mower

© Copyright by

Victor L. Ontiveros

2010

Acknowledgments

Support for this work was provided by the United States Nuclear Regulatory Commission (NRC). I would like to thank each project member for their continual support through out this research.

I would also like to thank the professors on my committee who have assisted me greatly through out my research by answering questions and offering guidance. Thank you Dr. Milke, Dr. Mowrer and Dr. Modarres for all of your help and advice.

I must also extend my great appreciation to Mr. Rick Peacock of the National Institute of Standards and Technology (NIST.) Mr. Peacock kindly responded to a torrent of emails, phone calls, and attended multiple meetings to help me understand the CFAST source code.

I would also like to thank the graduate students in the Reliability Engineering Program for their assistance. Specifically, I must thank Adrien Cartillier for his assistance throughout the project and Dr. Mohammadreza Azarkhail for introducing me to many of the tools used in this analysis.

Lastly I would like to thank my family and friends for their continual support.

Table of Contents

Acknowledgments.....	ii
Table of Contents.....	iii
List of Figures.....	vi
List of Tables.....	viii
Nomenclature.....	x
Chapter 1: Introduction.....	1
1.1 Motivation.....	1
1.2 Literature Review.....	3
Chapter 2: Inegrated Uncertainty Assessment Methodology.....	6
Chapter 3: Overview of Uncertainty Assessment Techniques.....	8
3.1 Phenomena Identification and Rankings Tables (PIRT).....	8
3.2 Input Uncertainty.....	11
3.3 Bayesian Inference.....	12
3.3.1 Sub-model Parameter Estimation using a Bayesian Inference.....	13
3.3.2 Output Updating using a Bayesian Inference (Black-Box Approach).....	14
3.3.3 Bayesian Inference (White-Box Approach).....	16
3.4 Wilks Tolerance Limit.....	18

Chapter 4: Sub-Model Uncertainty Characterization Example, Flame Height Sub-Model in the CFAST Code.....	20
4.1 PIRT	22
4.2 Sub-model Parameter Uncertainty	29
4.3 Input Uncertainties.....	32
4.4 Output Updating.....	33
4.5 Overall White-Box Methodology Uncerainty Results.....	35
Chapter 5: Sub-model Uncertainty Characterization Exxample, Plume Mass Flow in the CFAST Code.....	39
5.1 PIRT	40
5.2 Sub-model Parameter Uncertainty	43
5.3 Input Uncertainties.....	48
5.4 Output Updating.....	49
5.5 White-Box Uncertainty Results	50
5.6 Propagation of Results	56
Chapter 6: Conclusions	59
6.1 Future Research	60
Appendix A: Summary Statistics.....	62
Appendix B: Data	63
Appendix C: Computer Codes	67

Bibliography: 78

List of Figures

Figure 1-1: Black-box approach to model uncertainty	2
Figure 1-2: White-box approach to model uncertainty.....	2
Figure 3-1: Modified PIRT	11
Figure 3-2: Bayesian Inference Framework	12
Figure 4-1: ICFMP BE2.....	24
Figure 4-2: ICFMP BE3.....	25
Figure 4-3 : Historical flame height data	29
Figure 4-4 : Flame height equation comparison	30
Figure 4-5 : White-box mean values used in black-box model flame height results.....	36
Figure 4-6 : Black-box flame height results	37
Figure 4-7 : Explanation of results.....	38
Figure 5-1 : Far field plume mass flow apparatus	41
Figure 5-2: Near field plume mass flow apparatus.....	42
Figure 5-3 : Plume Centerline Velocity (a) and Temperature Rise (b).....	43
Figure 5-4 : White-box mean results in black-box model, Flame region, Plume mass flow rate	51
Figure 5-5 : Black-box flame region plume mass flow rate results.....	52
Figure 5-6 : White-box mean results in black-box model, Plume region, Plume mass	

flow rate	53
Figure 5-7: Black-box model results, Plume region, Plume mass flow rate.....	54
Figure 5-8 : Black-box intermittent region plume mass flow rate results	55
Figure 5-9 : White-box mean values used in black-box model, Intermittent region, Plume mass flow rate	55
Figure 5-10 : Code Structure, plume mass flow to HGL temperature calculation	57

List of Tables

Table 3-1: Two-sided quartile minimum sample size.....	19
Table 4-1: Realistic ranges of parameters.....	28
Table 4-2: Realistic variation non-dimensional parameter N.....	28
Table 4-3: Flame height parameter summary statistics	31
Table 4-4: HRR uncertainties	32
Table 4-5: Flame height expanded uncertainties	34
Table 4-6: White-box mean model predictions and experimental results	35
Table 4-7: White-box mean summary statistics, Flame height.....	35
Table 4-8: Black-box summary statistics, Flame height.....	36
Table 5-1: Plume mass flow equations.....	50
Table 5-2: Flame Region Summary Statistics using white-box mean.....	50
Table 5-3: Intermittent Region Summary Statistics using white-box mean.....	50
Table 5-4: Plume Region Summary Statistics using white-box mean	51
Table 5-5: Black-box flame region plume mass flow summary statistics.....	53
Table 5-6: Black-box intermittent region plume mass flow summary statistics	53
Table 5-7: Black-box plume region plume mass flow summary statistics.....	53
Table A-1: Black-box/White-box summary statistics, Flame height.....	62
Table A-2: Black-box/White-box summary statistics, Plume mass flow	62

Table B-1: Black-box model predictions and experimental results.....	63
Table B-2: White-box mean model predictions and experimental results.....	63
Table B-3: Black-box model predictions and experimental results, flame region	64
Table B-4: Black-box model predictions and experimental results, intermittent region..	64
Table B-5: Black-box model predictions and experimental results, plume region.....	65
Table B-6: White-box mean model predictions and experimental results, flume region .	65
Table B-7: White-box mean model predictions and experimental results, flume region .	66
Table B-8: White-box mean model predictions and experimental results, flume region .	66

Nomenclature

- a : normalized centerline temperature rise
- α : empirical equation parameter
- A_n : coefficient of centerline velocity variation
- β : empirical equation parameter
- β_w : probability of unknown distribution for Wilks Tolerance Limit Sampling
- B_n : coefficient of centerline temperature rise variation
- b_e : mean, error of experimental to the real value
- b_f : characteristic radius related to flame region
- b_m : mean, error of model to the real value
- C_B : local buoyancy constant
- c_p : specific heat
- C_λ : constant of integration, function of λ
- D : source diameter
- ΔE : difference between the initial and peak in experiment
- ΔM : difference of the initial and peak in model prediction
- E_{ik} : evidence
- F_e : multiplicative error of experiment to the real value
- F_i : multiplicative error of experiment to model prediction
- F_m : multiplicative error of model to the real value
- $f(\theta|Data)$: the posterior joint distribution of parameters
- $f_o(\theta)$: prior joint distribution of parameters
- γ : empirical equation parameter

γ_w : quantile of unknown distribution for Wilks Tolerance Limit Sampling
 g : acceleration of gravity
 ΔH_c : heat of combustion per unit mass of source fuel
 I_λ : analytical function of a
 K : entrainment constant from Equation 16
 K_λ : analytical function of a
 $L(.)$: likelihood function
 $LN(.)$: lognormal distribution function
 λ : ratio of thermal velocity width
 \dot{m}_c : total mass flow rate to the ceiling
 \dot{m}_f : fuel consumption rate
 \dot{m}_i : mass entrained at the interface between the upper HGL and lower cool air
 \dot{m}_{pl} : mass flow of the plume
 $\dot{m}_{e,air}$: mass of entrained air below the flame tip
 \dot{m}_r : mass entrained where the plume impinges upon the upper HGL
 m : number of test series
 M : local momentum flux
 M_k^s : number of model predictions made for the k'th experiment
 n_i : number of experiments in a respective test series
 n : exponent of centerline velocity and temperature rise variation with height
 N : nondimensional parameter defined in Equation 15
 N^s : number of experiments

N_w : minimum samples size for Wilks Tolerance Limit Sampling
 \dot{Q}_c : convective portion of heat release rate
 \dot{Q} : total heat release rate
 ρ_∞ : ambient density of air
 ρ_f : characteristic density
 r : mass stoichiometric ratio or air to source fuel
 s_e : standard deviation, error of experimental to the real value prediction
 s_m : standard deviation, error of model to the real value
 σ_v : 1/e width of radial profiles
 ΔT_f : maximum temperature rise above ambient in the flame region
 T_∞ : ambient temperature
 θ : the vector of parameters
 U : centerline vertical velocity
 u_e : absolute uncertainty of experiment
 \tilde{u}_e : relative uncertainty of experiment
 u_f : characteristic velocity
 \tilde{U}_e : expanded relative uncertainty of experiment
 $U_{c,E}$: weighted expanded combined measurement uncertainty
 ω : hyper-distribution of parameters
 $x_{1/e}$: characteristic width for both the plume velocity and temperature rise
 X : real quantity of interest
 X_e : result of experiment

- X_m : model prediction
- X_i : independent variable
- Y_i : dependent Variable
- z_f : flame height
- z : interface height between plume and smoke layer

Chapter 1: Introduction

1.1 Motivation

In 2004 the Nuclear Regulator Commission (NRC) amended Title 10, Section 50.48 of the Code of Federal Regulation (10 CFR 50.48) [1] to allow for reactor licensees to follow the recommendations of the National Fire Protection Association (NFPA) standard NFPA 805 [2] as opposed to existing deterministic fire protection requirements. NFPA 805 outlines the steps to be taken following a more risk-informed (RI)/performance-based (PB) method of fire protection. Fire simulation codes are powerful tools for use in a RI/PB approach. NFPA 805 allows for the use of simulation codes that are both acceptable to the Authority Having Jurisdiction (AHJ) and have undergone a verification and validation to ensure they reliably model the results of a fire.

A Verification and Validation [3] (V&V) for five popular fire simulation codes was performed in a joint effort between the NRC and the Electric Power Research Institute (EPRI.) In NUREG-1824 the experimental measurement uncertainty was estimated for a number of fire phenomena. Using the data provided in NUREG-1824, experimental results, simulation code predictions and estimates of experimental uncertainty, research performed at the University of Maryland (UMD) [4] resulted in an estimation of the total code output uncertainty. This methodology followed a “black-box” approach in which no consideration of the uncertainties associated with the inner workings of the code was considered. The black-box approach is presented graphically in Figure 1-1.

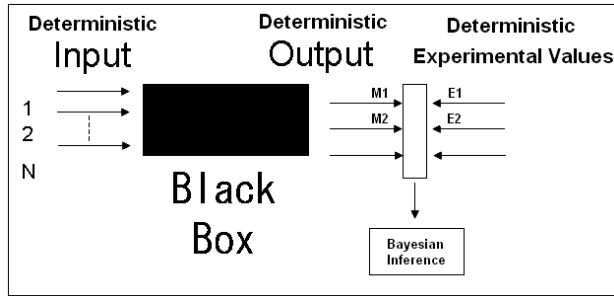


Figure 1-1: Black-box approach to model uncertainty

The work presented in this thesis represents the continuing research conducted at UMD on the basis of model (code) uncertainty. In this work a methodology capable of opening up a fire simulation code following a “white-box” uncertainty analysis is presented. In this white-box approach the uncertainties associated with inputs, sub-models and sub-model parameters are considered. The white-box concept is presented graphically in Figure 1-2. Similar to the black-box approach, a comparison of the simulation code output with experimental results is also considered in this approach.

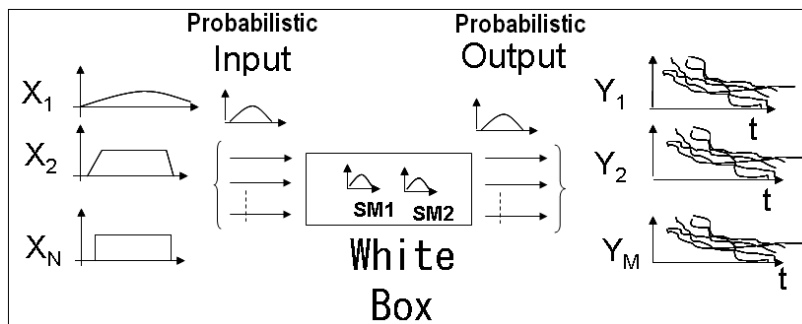


Figure 1-2 White-box approach to model uncertainty

The label white-box should not infer that a consideration of “every” possible uncertainty is captured in this analysis. Similarly, the black-box approach does not suggest that absolutely no consideration of the models inner works is made. Both designations are used to differentiate the level of analysis performed. A black-box analysis is a review of a

system with interest primarily on the output, while a white-box analysis is similar, but with the added knowledge and consideration of a systems inner workings.

Some of the sub-models within the fire simulation code CFAST (Consolidated Fire Growth and Smoke Transport Model) [5] of the National Institute of Standards and Technology (NIST) will be used as examples to show the application of the presented methodology. In particular, two sub-models, those used to calculate the flame height and plume mass flow/entrainment, will be presented to show the steps and results of the methodology. The simple flame height sub-model will be reviewed to show the application of the white-box approach. The plume mass flow/entrainment sub-model will be used to introduce the propagation of uncertainties throughout the calculations of the complex code structure. The simulation code output results from the white-box approach for both sub-models will be updated using experimental results following a similar method presented in the previous black-box research [4].

1.2 Literature Review

Bayesian methods for estimating model uncertainty have been suggested in previous research. One such example can be found in a dissertation by a previous student at the University of Maryland. In his dissertation [6], Droguett outlines multiple likelihood functions to be used in a Bayesian framework for estimating model uncertainty given different data sets. In his work he outlines a likelihood to be used for “Directly measurable Quantity, Performance Data as Descriptive/Predictive Model Error with Experimental Error” :

$$L(E_i | b_1, b_2, \sigma_1, \sigma_2) = \frac{1}{\sqrt{2\pi} \sqrt{\sigma_1^2 + \sigma_2^2}} e^{-\frac{1}{2} \left(\frac{E_i - (b_1 - b_2)}{\sqrt{\sigma_1^2 + \sigma_2^2}} \right)^2} \quad (1)$$

This generalized likelihood presented by Droguett was applied in the initial “black-box” methodology performed at UMD [4]. In his dissertation, Droguett also suggests a very generalized posterior for a “non-homogeneous” set of performance data that is more applicable to the research presented in this thesis.

A very similar posterior for non-homogeneous data is presented in a dissertation by another UMD student, Dr. Calvin Shirazi [7]. The goal of Shirazi’s work was to supplement insufficient data with expert judgment. Shirazi also used a Bayesian framework in his analysis and arrived at a very similar posterior to that proposed by Drougett. This posterior, while very similar to that presented by Drougett, accounts for a “hybrid” set of performance data. As presented in his dissertation, Shirzai explains a hybrid, or mixed, set of data as resulting from a situation in which there were multiple estimates for a single “true” value. Following the methodology presented in this thesis, a hybrid set of data is expected to result in a distribution of simulation predictions to be paired with a single experimental measurement. Later in this thesis, Shirazi’s posterior will be reviewed in depth for application in this methodology.

A third dissertation by a UMD student was reviewed in preparation for this research in the hopes of finding common ground. In his dissertation, Pourgol-Mohamad undertakes a similar task of estimating the uncertainty of thermal-hydraulic simulation codes [8]. The work by Pourgol-Mohamad was used as guidance, since the challenges resulting from this analysis were expected to be similar. Most notably gained from reviewing Pourgol-Mohamad’s work are the inclusion of the Phenomena Identification and Ranking Table (PIRT) and Wilks Tolerance Limit, both of which will be reviewed later in this analysis. A major difference between this research and that of Pourgol-Mohamad is that in this work

multiple different experimental measurements, from different test series, are used resulting in a wide ranging estimation of the model uncertainty to be made for a more general use. In the work by Pourgol-Mohamad, this does not appear to be the case. Therefore, the Bayesian framework used between the two methods is different.

Chapter 2: Integrated Uncertainty Assessment Methodology

The goal of this research is to build upon previous work [4] and present a more complete methodology for estimating the uncertainties resulting from the predictions of a fire simulation code. To do this, multiple sources of uncertainty must be considered. These sources include uncertainties associated with the simulation code inputs, uncertainties associated with the use of different sub-models within the simulation code and sub-model parameter uncertainties.

To include and account for different sources of uncertainties, this methodology follows a number of steps outlined below.

1. Phenomena Identification and Ranking Table (PIRT) Development: This table is used to identify and rank different phenomena considered in the simulation code. The primary objective of this tool is to bring into focus those phenomena that most significantly influence the output. This is an important step for two reasons. First, as more and more phenomena are identified it will quickly become unrealistic to account for each and every one. Second, not every phenomenon is as important as another. Some phenomena may not be as influential on the overall results when compared to others. Similarly, it may be determined that the influence of a phenomena is so small it can be taken to be negligible.

2. Input Uncertainties Consideration: Using data reported from experimental reports, probability distribution functions (pdf's) for inputs are developed. In some cases, especially when considering older experiments, information pertaining to the error of measurements is not discussed or considered in the reports. In such cases, expert judgment, given previous experience with similar testing scenarios and equipment, can be used.

3. Assessment of Sub-model Parameter Uncertainties: The pdf's for sub-model parameters are developed given the historical data used to derive the original equations. A Bayesian regression technique is used to perform this step. This not only allows for an estimation of the joint pdf of the parameters used in the sub-models, but also provides an estimation of their respective confidence intervals.

4. Use of Wilks Tolerance Limit Sampling: As a result of the white-box approach, the simulation code no longer predicts a single value but a pdf of output results. In this distribution the uncertainties within the sub-model and inputs to the simulation code are captured. This results in a question as to the number of samples required to fully capture the total distribution of error. The Wilks Tolerance Limit Sampling technique stipulates the number of simulations required to account for a chosen percentage of the pdf observed for a desired confidence interval.

5. Perform Bayesian Output Updating: The code output prediction pdf's are further updated with experimental results using a Bayesian estimation algorithm. This step helps account for uncertainties not captured in the inclusion of input uncertainties, sub-model parameter uncertainties and those eliminated in the PIRT. Uncertainties not considered, such as those resulting from an inadequate sub-model and numerical calculations are accounted for in this process.

Chapter 3: Overview of Uncertainty Assessment Techniques

3.1 Phenomena Identification and Ranking Table (PIRT)

Originally developed [9,10,11] as a “Best-Estimate (BE) plus uncertainty licensing” option for use in the Code Scaling And Uncertainty (CSAU) [9] evaluation methodology, the PIRT process was found to be an excellent tool for use in computer code safety analysis. Wilson and Boyack [12] describe the steps of a typical PIRT process. These steps are summarized below:

1. Define problem and objectives of the process.
2. Define plant designs and the scenarios.
3. Define parameters of interest.
4. Identify, obtain and review all available data.
5. Partition transient scenario into convenient time phases and plant design into and components.
6. Identify plausible phenomena by phase and component
7. Develop a ranking for identified components and phenomena by expert judgment and discussions, or by using pair-wise AHP methodology.
8. Perform sensitivity analysis to confirm the results from the previous steps.

In applying the PIRT process for use with fire simulation code uncertainty analysis, some steps may differ slightly from that of a purely traditional approach. One example of this difference can be seen in the focus on the plant design. In applications with fire simulation codes, the fire compartment may be a better identifier to be used in the PIRT process. Since the PIRT is dependent on the overall objective, these semantic differences should not be seen

necessarily as a change in the PIRT process application, but more as specialization of focus determined by the over all PIRT objective.

Other noticeable differences between the applications of the PIRT process in this methodology compared with the traditional approach are in the steps involving transient scenarios and time phases. Building on the previous uncertainty work [4] and the information provided in NUREG-1824 [3] all data is reduced to “ordered pairs” of a maximum model (code) prediction and maximum experimental result. This decision eliminates all temporal information rendering steps specific to time phases unnecessary.

The fourth step, obtain and review all available data, is an especially important one in the PIRT process. This methodology makes extensive use of historical data and experimental results in almost every phase. Therefore, determining what and how applicable available data is, becomes a very vital step of the PIRT process.

Traditionally, the term “phenomena” is considered to mean any “phenomena, process, component function, behavior, condition or status” with respect to a user defined figure of merit. For use with fire simulation code uncertainty analysis the term phenomena will most often be used to mean physical fire phenomena such as temperature, radiation, mass flow, etc.

After an objective has been defined and phenomena have been identified, these phenomena are ranked by judgment according to their importance with respect to the objective of the PIRT. This ranking can be done either by an informal expert judgment process or through the use of a more robust technique. Commonly, the Analytic Hierarchy Process (AHP) [13] is used as a formal approach to ranking identified phenomena. The AHP process was developed to provide a systematic approach for reducing multi-objective complex decisions into smaller more manageable pair-wise decisions. As more and more

phenomena are identified it can become increasingly difficult to decide which phenomena are the most important when judged against one another. This is especially true when multiple experts are involved. In reducing decisions to pair-wise comparisons, decisions become simpler, making the AHP process an excellent tool for use in the PIRT process. The ranking performed as part of the PIRT process, by use of the AHP method or not, can be done qualitatively, describing importance as high, medium and low or quantitatively with a ranking from 1 to 9, where the value of 9 is attributed to phenomena of the highest importance, and 1 pertains to the lowest.

The examples presented in this thesis did not result in the identification of large numbers of phenomena. Therefore, the AHP method did not become necessary for use in the examples presented later, but is included to provide a formal technique to ranking phenomena, should it become necessary.

One final difference between the PIRT process applied in this methodology compared to a more traditional PIRT is to perform a second ranking step to consider the importance of the uncertainty in phenomena identified. The PIRT process used in this methodology will follow the concept of a two-step “Modified PIRT” as described by Pourgol-Mohamad [8] for applications to thermal hydraulics code uncertainty assessment. This modified PIRT is first conducted considering the phenomena’s influence on the simulation codes output. Then, in a second step, the phenomena are ranked a second time on the basis of the importance of uncertainty of the phenomena. Phenomena identified as critical are those that are determined to be important not only with respect to the outcome of the model (code) prediction, but also as a result of uncertainty in phenomena. This is depicted graphically in Figure 3-1.

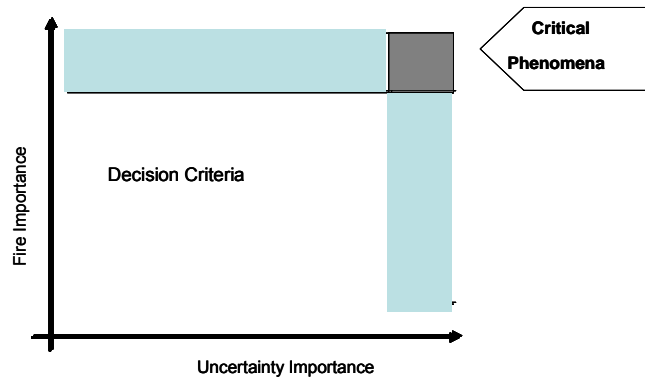


Figure 3-1: Modified PIRT [8]

A recent PIRT [14] analysis with respect to fire modeling was performed on behalf of the U.S. NRC Office of Nuclear Regulatory Research and facilitated by Sandia National Laboratories. In this PIRT, a group of experts were presented with different fire specific scenarios relatable to typical nuclear power plant scenarios. For the purpose of this research, the results of the PIRT performed for the NRC were not found to be significantly relatable. However, in keeping with the fourth step described in the general PIRT process, all available data should be identified, reviewed and considered.

3.2 Input Uncertainty

Uncertainties in the values used as input for a simulation code are propagated in the simulation code to find the effects on the output uncertainty. Thus, to arrive at the best possible overall estimation of uncertainty, the uncertainty of inputs must be considered and estimated.

In this methodology input uncertainties are developed using the available information reported from experiments or other sources of information. These experiments are the same as those that will be used to compare with the model in the output updating stage of the methodology. For cases in which uncertainty is not reported, expert judgment given prior

experience with similar experiments and test equipment can be used to develop a probability distribution function for the inputs.

As will be seen in the second example, most simulation codes are complex, consisting of multiple sub-models. For this reason in many cases the results from a sub-model will be used as inputs in other sub-models.

3.3 Bayesian Inference

The Bayesian inference is a technique used to update a given “state of knowledge.” In the Bayesian inference a subjective prior pdf of parameters $f_0(\theta)$ is combined with observed data (evidence) in the form of a likelihood function of an unknown parameter θ . The result is an updated state of knowledge in the form of a posterior pdf, $f(\theta|Data)$. This process is shown mathematically in Equation 2. The Bayesian framework is outlined below in Figure 3-2.

$$f(\theta | Data) = \frac{L(DATA|\theta) f_0(\theta)}{\int_{\theta} L(DATA|\theta) f_0(\theta) d\theta} \quad (2)$$

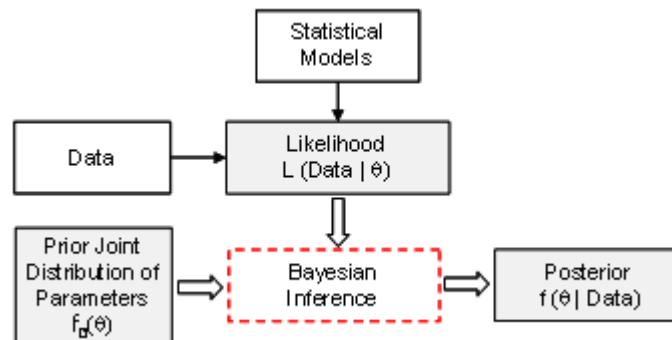


Figure 3-2 Bayesian Inference Framework [16]

In this research the Bayesian inference is solved using the program WinBUGS [15]. This program has been used in previous parameter estimation research [16] and output updating analysis [4,8]. For more information on WinBUGS see Cowles [17.]

A Bayesian inference approach is used for two purposes in the presented methodology. The tool is used initially to develop pdf(s) over sub-model parameters given the historical data used to derive the equation. A Bayesian inference is used a second time to update the simulation code predictions with experimental results following a likelihood function similar to that developed in the previous black-box research performed at the University of Maryland [4].

3.3.1 Sub-model Parameter Estimation using a Bayesian Inference

Within the deterministic simulation codes, sub-model parameters are often considered constants. However, in most cases these “constants” are fit from historical data. By considering these parameters constant, the uncertainty represented by the scatter of data used to develop the sub-models, is lost. To account for this error, and better capture to full range of possible simulation code predictions, pdf(s) over these sub-model parameters are developed given the historical data used to develop the sub-models. This work is done following a Bayesian inference. In this thesis the uncertainty due to scatter of data in the historical data, is assumed normally distributed. The assumption of a normal distribution in the scatter of experimental results is a common assumption made [18], but given expert judgment, other pdf’s may be used. The data is represented in the form of a likelihood function based on a normal distribution, and combined with a subjective prior distribution. Prior pdf(s) are developed around the historical values of a sub-model parameter. The resulting posterior pdf best captures the possible sub-model parameter values given the available data. The posterior pdf is also bounded with a confidence interval.

The general form of the normal likelihood function used in the sub-model parameter uncertainty steps is shown below:

$$L(Data | \theta) = \prod_{i=1}^n \frac{1}{\sqrt{2\pi}\sigma} e^{-\frac{1}{2} \times \frac{[Y_i - f(X_i)]^2}{\sigma^2}} \quad (3)$$

where Y_i is the dependent variable and X_i is the independent variable of the sub-model function $Y=f(X; \theta)$.

This likelihood is combined with the pdf(s) developed to represent the prior state of knowledge resulting in estimation of the posterior as described by Equation 2.

3.3.2 Output Updating using a Bayesian Inference (Black-Box Approach)

The Bayesian inference is used a second time in the methodology to update the model predictions with experimental results. Output updating with independent experimental results (results not used as historical values to update sub-model parameters) helps account for uncertainties not captured in the distributions developed for inputs and sub-model parameters. These uncertainties can be the result of incomplete sub-models incapable of fully capturing all phenomena of the parameter being measured, uncertainties excluded in the PIRT process or numerical uncertainties.

Just as in the black-box research [4] the assumption that the error associated with the experimental measurements is independent to that of the error resulting in the simulation code predictions is made. In the black-box research the fire phenomena studied, each had experimental uncertainties provided in the form of a relative or percentage error [3]. In this white-box approach the experimental uncertainties will often not be directly provided. In such cases, experimental uncertainties will need to be determined. More often than not, in the

presentation of experimental results, little or no discussion of measurement uncertainty is presented. In these cases, uncertainties will need to be developed using expert judgment, given prior experience with similar testing scenarios and equipment. For cases in which there is no reliable prior experience or similar scenarios, expert judgment can still be used. However, it should be done understanding that with little or no reliable experience, the uncertainty resulting from such a decision could be considerable. The uncertainties to be used are those of the “relative expanded uncertainties” resulting from measurements, \tilde{U}_E . Using the relative expanded uncertainties from each experimental test set, experimental uncertainties used in this study are determined following the method described in NUREG-1824 [3] by use of calculating the weighted expanded combined uncertainty defined in Equation 4:

$$U_{c,E} = \frac{1}{\sum_{i=1}^m n_i} \sum_{i=1}^m \tilde{U}_E n_i \quad (4)$$

where m is the number of test series and n_i is the number of tests in a respective test series. $U_{c,E}$ is the experimental uncertainty to be used in the output updating step for estimating the model uncertainty. For more information on the determination of experimental measurement uncertainties see NUREG-1824 [3].

Reviewing the black-box methodology, both the model (code) prediction and experimental result are considered to be estimations of physical reality of interest, given some error as shown in Equations 5 and 6.

$$\frac{X_i}{X_{e,i}} = F_{e,i} \quad ; \quad F_e \sim LN(b_e, s_e) \quad (5)$$

$$\frac{X_i}{X_{m,i}} = F_{m,i} \quad ; \quad F_m \sim LN(b_m, s_m) \quad (6)$$

where X_i is reality, $X_{e,i}$ is the experimental result, $X_{m,i}$ is the model prediction, F_e is the multiplicative error of experiment with respect to reality, and F_m is the multiplicative error of the model prediction, with respect to reality.

Combining Equations 5 and 6, the result is:

$$\begin{aligned} F_{e,i} X_{e,i} &= F_{m,i} X_{m,i} \\ \frac{X_{e,i}}{X_{m,i}} &= \frac{F_{m,i}}{F_{e,i}} = F_{t,i} \end{aligned}$$

Assuming Independency of F_m, F_e then,

$$F_t \sim LN\left(b_m - b_e, \sqrt{s_m^2 + s_e^2}\right) \quad (7)$$

where F_t is the multiplicative error of experiment with respect to the model prediction.

3.3.3 Bayesian Inference (White-Box Approach)

In this research, as a result of the white-box methodology presented, $F_{t,i}$ discussed earlier will no longer be a single ratio, but a pdf resulting from the combination of multiple simulation code runs paired with a single experimental result. Thus, a one-to-one comparison, as seen in the black-box methodology, is not applicable. To account for this new distribution, F_t will need to be multiplied by the pdf of model predictions and integrated over each distribution resulting from independent cases as described in Equation 8.

$$F_t \sim \int_{b_m, s_m} LN\left(b_m - b_e, \sqrt{s_m^2 + s_e^2}\right) \cdot g(b_m, s_m) db_m ds_m \quad (8)$$

where $g(b_m, s_m)$ is the joint probability distribution function of parameters b_m and s_m .

The resulting posterior of this analysis is a bit more complex than that performed in the black-box analysis. The idea of unpaired, hybrid, data has been considered in previous uncertainty analysis work. Shirazi [7] proposes a posterior for use in dealing with expert

judgment. In his research multiple estimations by experts are compared to a single “true value.” By considering the multiple estimations made by experts as the multiple model (code) predictions and the true value to be the same as the experimental result, Shirazi’s posterior can be used in this research.

In the case involving multiple estimates for one true value, the parameters, θ , of the distribution of error are themselves probability distribution functions. Shirazi defines this variability of $f(\theta)$ as a set of “hyper-parameters”, $\omega(\omega_1 \dots \omega_n)$ making the distribution of error, $f(\theta | \omega)$.

Given this description, the desired posterior distribution of error given the evidence becomes the expected, or average distribution:

$$\bar{f}(b_m, s_m | X_{e,k}, X_{m,i}, b_e, s_e) = \int_{\omega} f(b_m, s_m | \omega) \pi(\omega | X_{e,k}, X_{m,i}, b_e, s_e) d\omega \quad (9)$$

The resulting posterior specific to this analysis becomes:

$$f(b_m, s_m | X_{e,k}, X_{m,i}, b_e, s_e) = \int_{\omega} f(b_m, s_m | \omega) \frac{\prod_{k=1}^{N^s} \left(\prod_{i=1}^{M_k^s} \int_{b_m, s_m} L(X_{e,k}, X_{m,i}, b_e, s_e | b_m, s_m) f(b_m, s_m | \omega) db_m ds_m \right) \pi_o(\omega)}{\prod_{k=1}^{N^s} \left(\prod_{i=1}^{M_k^s} \int_{b_m, s_m} L(X_{e,k}, X_{m,i}, b_e, s_e | b_m, s_m) f(b_m, s_m | \omega) db_m ds_m \right) \pi_o(\omega)} d\omega \quad (10)$$

where N^s experiments will be updated with M_k^s model predictions of the k’th experiment.

The likelihood to be used with Equation 10 will be the same as presented in the black-box analysis [4]:

$$L(X_{e,i}, X_{m,i}, b_e, s_e | b_m, s_m) =$$

$$\prod_{i=1}^n \frac{1}{\sqrt{2\pi} \left(\frac{X_{e,i}}{X_{m,i}} \right) \sqrt{s_m^2 + s_e^2}} e^{-\frac{1}{2} \times \frac{\left[\ln \left(\frac{X_{e,i}}{X_{m,i}} \right) - (b_m - b_e) \right]^2}{s_m^2 + s_e^2}} \quad (11)$$

The experimental results are uncertain, with a given error as defined in Equation 5. WinBUGs is not capable of solving the complex posterior described in Equation 10. Therefore, in this analysis, the distribution of model predictions will be reduced to a mean value and compared one-to-one with the experimental results following the black-box approach. This approach, while not ideal, provides a quick estimation of the uncertainty. By using only the mean value of a model prediction the scatter of the results is lost.

3.4 Wilks Tolerance Limit

To propagate uncertainty from inputs, sub-model parameters and sub-model results, multiple samples from respective distributions and simulation code runs will be needed. The Wilks Tolerance Limit Sampling method describes how the samples required to capture the desired distribution can be less than 100 samples, as opposed to thousands. From work pioneered by Wilks [19, 20] and Wald [21, 22, 23], the tolerance limit method is used to ensure the interval produced contains a desired fraction of the population γ_w , with a probability of β_w .

As described by Guba et al. [24] letting the probability of a single output failing to be in the goal group N_w be represented by γ_w , the probability of all outputs failing to be in the goal group is $\gamma_w^{N_w}$. By this definition, the probability of obtaining at least one success is:

$$\beta_w = 1 - \gamma_w^{N_w} \quad (12)$$

Equation 12 can be used to find the sample size required for a one-sided quantile. A one-sided quantile is commonly used in risk assessment, as information about the lower limit is often not desired. In this methodology two-sided quartiles will be considered given the previous work on uncertainty bounds. The formulation of β_w [25] for a two-sided quartile is defined as:

$$\beta_w = 1 - \gamma_w^{N_w} - N_w(1 - \gamma_w)\gamma_w^{N_w-1} \quad (13)$$

The result is an estimation of the number of samples, N_w required to capture a desired portion of the population, γ_w , with a probability of β_w shown in Table 3-1.

Table 3-1: Two-sided quartile minimum sample size

$\beta_w \rightarrow$	0.5	0.9	0.95	0.99
$\gamma_w \downarrow$				
0.5	3	17	34	163
0.8	5	29	59	229
0.9	7	38	77	388
0.95	8	46	93	473
0.99	11	64	130	663

For more on the Wilks Tolerance Limit sampling criteria see Pal and Makai [26,27].

Chapter 4: Sub-Model Uncertainty Characterization Example, Flame Height

Sub-Model in the CFAST Code

In the first example the sub-model used to calculate the flame height in the fire simulation code CFAST will be studied. The flame height is calculated in CFAST by the routine `heskestad.f90` following the equation developed by Heskestad [28] shown below.

$$z_f = -1.02D + 0.235\dot{Q}^{2/5} \quad (14)$$

where z_f is the flame height, D is the source diameters, and \dot{Q} is the total heat release rate (HRR).

Heskestad [29] developed his global model for correlating flame-height data following work on predicting the maximum gas velocities within a buoyancy-controlled turbulent diffusion flame.

Assuming infinite kinetics, the flame is expected to extend to a height at which the total air entrained becomes just enough to complete combustion. This results in the following relation:

$$\dot{m}_{e,air} = \dot{m}r \quad (15)$$

where $\dot{m}_{e,air}$ is the mass of entrained air below the flame tip, \dot{m} is the mass pyrolysis rate, and r is the stoichiometric mass ratio of air to volatiles.

The total entrainment rate of air is determined using a relation for local entrainment rates in jets given different surrounding densities by Ricou and Spalding [30].

$$\frac{d\dot{m}_i}{dz} = K(M\rho_\infty)^{1/2} \quad (16)$$

where K is an entrainment constant, M is the local momentum flux, and r is the stoichiometric mass ratio of air to volatiles. The resulting estimation of the total entrainment rate from the base of the fire to the flame tip, z_f is determined following:

$$\dot{m} = \int_0^{z_f} \left(\frac{d\dot{m}_i}{dz} \right) dz \approx K \cdot z_f \left(\rho_f \cdot u_f^2 \cdot b_f^2 \cdot \rho_\infty \right)^{1/2} \quad (17)$$

where ρ_f is characteristic density, u_f is a characteristic velocity, and b_f is a characteristic radius related to the flame region. From his work with gas velocities Heskestad proposed a relation between b_f and the convective heat release rate, \dot{Q}_c :

$$b_f = \left(\frac{\dot{Q}_c}{c_p \cdot \rho_f \cdot u_f \cdot \Delta T_f} \right)^{1/2} \quad (18)$$

where ΔT_f is the maximum temperature rise above ambient in the flame region.

Using relations for the characteristic velocity, convective heat flux, and maximum temperature rise above ambient in the flame region, Heskestad arrives at a relation for the length of the flame:

$$\frac{z_f}{D} = fn \left(\frac{c_p T_\infty}{g \rho_\infty^2 \alpha} \frac{\dot{m}^2 r^3}{H_c D^5} \right) \quad (19)$$

where c_p is the specific heat, T_∞ is the ambient temperature, g is the acceleration due to gravity, ρ_∞ is the ambient density, H_c is the heat of combustion, and r is the mass stoichiometric ratio of air to fuel, and α is the convective fraction of the total heat release rate.

Using this relationship and extensive data, Heskestad developed a general equation for determining the flame height [31]:

$$\frac{z_f}{D} = -1.02 + 15.6N^{1/5} \quad (20)$$

where:

$$N = \left[\frac{c_p T_\infty}{g \rho_\infty^2 \left(\frac{H_c}{r} \right)^3} \right] \left(\frac{\dot{Q}^2}{D^5} \right) \quad (21)$$

With this background knowledge of the equation used in CFAST, applying the methodology described above, the initial step is to perform a PIRT to determine the different sources of uncertainty to be accounted for.

4.1 PIRT

Traditionally a PIRT would be applied to an entire code, resulting in the ranking of multiple sub-models and consecutively, multiple parameters in an attempt to focus only on the phenomena most significant to the analysis. For the two examples presented in this work it would appear a full robust PIRT is unnecessary. However, to provide an example of the methodology, a simplified application will be described for completeness.

Following the outline of the PIRT process presented in section 3.1, the objective of this PIRT is to determine the phenomena significant to the flame height calculation performed in CFAST. The only limit placed on designs or scenarios will be to those of a typical nuclear power plant setting. This is done so as to lessen any limits on the data available for use in the analysis.

The phenomena of interest to calculate the flame height z_f , are the HRR \dot{Q} , the source diameter D , and the model parameter constants. Later in the analysis additional parameters are identified and should be ranked. These parameters include the acceleration due to gravity g , specific heat c_p , ambient temperature T_∞ , ambient density ρ_∞ , heat of

combustion H_c , and stoichiometric ratio of air to fuel r . A final phenomenon of interest is the energy lost in bringing the oxygen and fuel to the required lower heating value.

The data used in this PIRT will include experimental data of flame heights presented in NUREG-1824 [3], flame heights for the tests performed in Iceland by NIST [32], and the data used to develop the flame height equation used in CFAST [28].

The experimental results shared between this analysis and NUREG-1824 come from the International Collaborative Fire Model Project (ICFMP) Benchmark Exercise #2 and #3.

ICFMP Benchmark Exercise #2 (BE2) [33] test series was undertaken to provide data for use in zone model and CFD code verification, specifically data on smoke filling and the heating of steel structures. The tests were performed in the Valtion teknillinen tutkimuskeskus (VTT) Fire Test Hall in Finland between 1998 and 1999.

Of the 8 experiments performed only one test of the series was used in the analysis specific to this report, Test BE 2-2. BE2-2 was carried out in space 19m high x 27m long x 14m wide (Figure 4-1). The walls and ceiling of the space was made of layer of mineral wool under a 1 mm thick sheet metal layer. The floor of the compartment was made of concrete. During BE2-2 no doors were opened limiting any natural ventilation to that of leakage, suggested to be 2 m^2 by the scientists who conducted the experiments [3]. A maximum HRR of 3000~kW, calculated from the mass loss rate, was developed using a 1.6m diameter pan filled with heptane. For more information on this testing series see Hostikka [33].

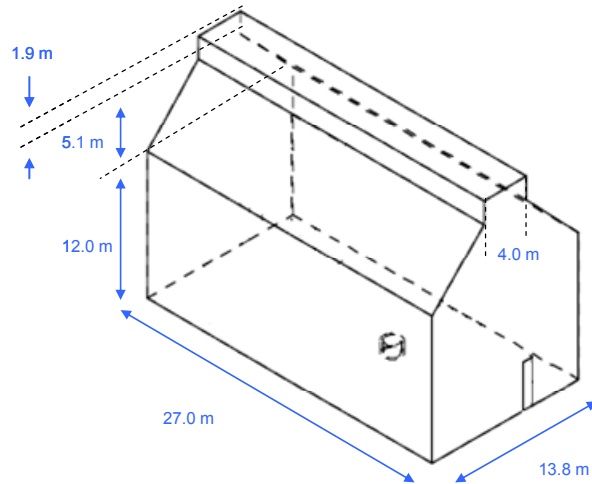


Figure 4-1: ICFMP BE2 [33]

Flame height was not a parameter measured in BE2-2. Instead, the flame height was determined using photographs taken during the testing periods at a later date. For this reason there is expected to be considerable experimental uncertainty associated with this measurement. This uncertainty will be discussed later.

ICFMP Benchmark Exercise #3 (BE3) [34] consisted of 15 experiments performed at NIST in June of 2003 for use in validating fire simulation computer codes for use in nuclear power plant applications. Once again, despite measuring numerous different phenomena including HGL temperature, HGL depth, ceiling jet temperature, heat flux, surface temperatures, etc., flame height was not a phenomena measured in this test series. Similar to BE2-2, the flame height for one test, BE3-3 was determined using photographs taken during the experiments at a later date.

Test BE3-3, the test for which the flame height value is taken and used in this analysis, took place in a 21.6 wide x 7.04 long x 3.82 m high space (Figure 4-2). The test compartment interior walls and ceiling were lined with two 12.5 mm layers of marine boards. The floor of the compartment was covered with a 12.5mm layer of gypsum board over a 18.3 m layer

of plywood. A door way of 2 m x 2 m was open during test BE3-3. A maximum HRR of 1190 kW determined using oxygen consumption calorimetry, was developed from a 1 diameter pan filled with heptane. For more information on this testing series see Hamins et al [34].

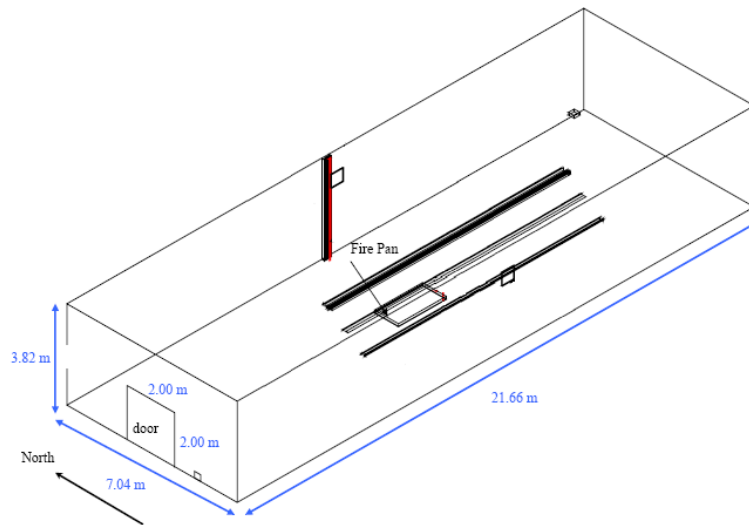


Figure 4-2: ICFMP BE3 [34]

Unfortunately, only two experimental measurements of flame height are gained from using these two tests series. Additional flame height measurements used in this analysis come from a test series performed by NIST.

The High Bay Hangar [32] tests performed by the Naval Facilities Engineering Command (NAVFAC) and NIST are a set of 33 individual experiments carried out in two different locations, Barber's Point, Hawaii and Keflavik, Iceland. Of these 33 tests, nine tests were used in this analysis. The nine tests used were all performed in Keflavik. A major difference between these High Bay tests and the previous test series is that the flame height was a value recorded for analysis. The High Bay tests were performed to determine how the

“latest generation of fire detectors” respond to fires, including smoke, heat, projected beam, and UV/IR optical flame detectors.

The hangar the tests were carried out in was approximately 73.8 m long x 45.7 m wide x 12.2-22.3m high ceiling. The hangar ceiling was arched. The hangar walls were constructed in a combination of concrete masonry units and gypsum board. Two ends of the hangar were constructed of metal and glass horizontal sliding doors. The roof of the hangar consisted of a metal deck attached to a number of primary and secondary steel trusses. Steel draft curtains separated the ceiling of the hangar into five equal basins approximately 14.8 m by 45.7 m. The curtains extend to a height of 13.4 above the floor. The steady state heat release rates ranged from 1.4-33 MW with varying pan sizes among the different experiments used in this analysis. HRRs were determined using mass loss rates. For more on the High Bay Tests see Gott [32]. Having identified the different phenomena inherent to the flame height sub-model used in the simulation code and experimental test data to be used in the analysis, the phenomena can now be ranked.

Often, the ranking of phenomena in a PIRT process will be done by a group of experts. In this analysis the ranking was performed by the author of this thesis with limited, informal, consultation of other experts. Phenomena were ranked with respect to their effect on the calculation of the flame height and the uncertainty in the knowledge of the phenomena following the two-step PIRT process described in section 3.1. Phenomena and parameters determined to rank low with respect to both the effect in the calculation and uncertainty are considered to be insignificant enough to be used as deterministic values or ignored.

An example of a low ranking phenomenon is the energy lost in bringing the oxygen and fuel to the required lower heating values. This phenomenon is calculated by the CFAST

routine PYROLS.f90. The effect on the final calculation and uncertainty contribution made by this routine was considered low enough to be ignored. Therefore, only the routine flamhgt.f90, the routine used to calculate the flame height, is considered for further analysis. Similarly, the effect and uncertainties in g , T_∞ , c_p and ρ_∞ were considered insignificant and left as deterministic values. The value of H_c/r , which changes with fuel, was considered to be significant enough to be sampled from a uniform distribution, given the ranges of value presented in the SFPE handbook derivation of Equation 14 [28].

\dot{Q} , D and the model parameter constants fit from the historical data are ranked high in terms of effect on the resulting calculation and uncertainty. Given the historical data used to formulate the equation used in CFAST and the data available from the specific experimental flame height tests, pdf's will be determined for these phenomena and parameters for use in the uncertainty analysis.

As stated in the description of the PIRT process, after phenomena are ranked by expert judgment, a sensitivity analysis is performed to ensure the phenomena that are important to the analysis are being considered.

A simple sensitivity analysis is performed so that the effects of variation can be observed. This will give an idea of how influential each parameter is with respect to the results.

Reviewing Heskestad's flame height equation, there are a number of parameters to vary. Expert judgment has only identified the (HRR) \dot{Q} , source diameter D , equation constants and the heat liberated per unit mass of air entering the combustion reaction, H_c/r as having a large enough effect on the result to consider any variation of the respective parameters. Therefore, this sensitivity analysis will be performed focusing on the other

parameters considered in the flame height equation to ensure that ignoring effects of their variation is a reasonable assumption.

Many of the parameters taking the focus of this analysis are lumped together in the non-dimensional parameters N of Equation 21. Within it, the term N accounts for the T_∞ , c_p , g and ρ_∞ .

In this analysis negative values will not be considered. This is done because it would be unrealistic to expect a negative density or gravity in any instance for which the results of this analysis could be considered.

The parameters will be varied within realistic ranges to confirm the applicability of the subjective expert rankings. This also helps to show realistic effects of varying the parameters under realistic conditions. Realistic ranges of the T_∞ , c_p , ρ_∞ are presented in Table 4-1.

Table 4-1: Realistic ranges of parameters [35]

Temperature (K)	Density (kg/m ³)	Specific Heat (kJ/kg-K)
273	1.293	1.005
293	1.205	1.005
313	1.127	1.005
333	1.067	1.009
353	1.000	1.009
373	0.946	1.009

The upper and lower values presented in the table will be used in the sensitivity analysis. Values of gravity for different cities, Oslo (9.819) and Mexico City (9.779) will be used to determine an applicable range of gravity to use [36].

Table 4-2: Realistic variation non-dimensional parameter N

Variation	$T_\infty/\rho/c_p$	g
Lower	0.271	0.235
Upper	0.228	0.235

Recalling that the original value of N was 0.235, it would appear that strong variations in T_∞ , ρ_∞ , and c_p could have a non-trivial effect on the calculation of the flame height. Following a more robust uncertainty analysis, the effect of varying these parameters should be considered.

With the focus squarely on the `flamhgt.f90` routine, and the phenomena associated with it, the next steps were to develop pdf's over input values, and sub-model parameters, to account for their respective uncertainties.

4.2 Sub-model Parameter Uncertainty

Starting with the sub-model parameters, distributions will be developed following the Bayesian curve fitting technique described in section 3.3.1.

The historical data shown in Figure 4-3, used to develop the flame height equation, is provided for in an alternate form of the equation used in CFAST, Equation 14.

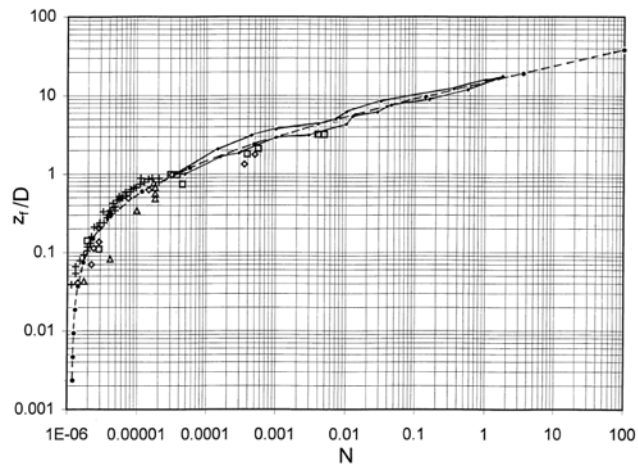


Figure 4-3: Historical flame height data [31]

To use this data in the Bayesian inference an empirical form of Equation 15 was used as shown below:

$$\frac{z_f}{D} = \alpha + \beta N^\gamma \quad (22)$$

Pairing the assumption of a normally distributed error with the empirical form of the equation the resulting posterior of the Bayesian framework is presented below:

$$f(\alpha, \beta, \gamma | z_f / D, N) = \frac{f_0(\alpha, \beta, \gamma) \times L(z_f / D, N | \alpha, \beta, \gamma)}{\int \int \int_{\alpha \beta \gamma} f_0(\alpha, \beta, \gamma) \times L(z_f / D, N | \alpha, \beta, \gamma, \sigma) d\alpha d\beta d\gamma} \quad (23)$$

where:

$$L(z_f / D, N | \alpha, \beta, \gamma, \sigma) = \prod_{i=1}^n \frac{1}{\sqrt{2\pi\sigma}} e^{-\frac{1}{2} \times \frac{[z_f / D - \alpha - \beta N^\gamma]^2}{\sigma}} \quad (24)$$

with $f_0(\alpha, \beta, \gamma)$, the joint prior pdf of parameters, and $f(\alpha, \beta, \gamma | z_f / D, N)$, the posterior joint pdf of parameters.

The result is a distribution over parameters α , β and γ , capturing the scatter seen in the historical data. Using the means of the distributions over α , β and γ , the resulting line of best fit is slightly different when compared to the historical equation. This difference is seen in Figure 4-4.

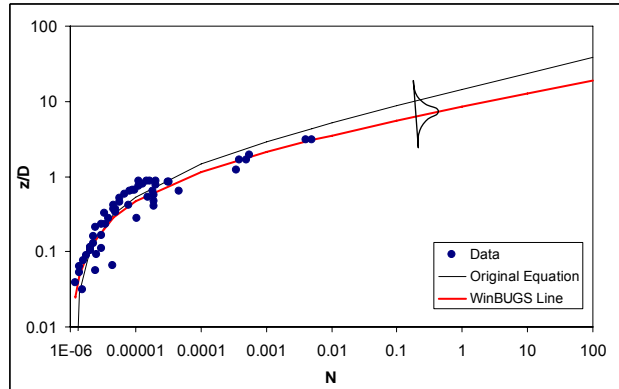


Figure 4-4: Flame height equation comparison

As the new line is a result of a distribution of parameters, the line has its own confidence bounds. The summary statistics of the parameters α , β and γ are shown in Table 4-3.

Table 4-3: Flame height parameter summary statistics

Parameter	Mean	SD	2.50%	Median	97.50%
α	-1.07	0.37	-1.87	-1.02	-0.47
β	9.52	0.81	8.35	9.39	11.49
γ	0.16	0.03	0.11	0.16	0.22

Recalling that the distributions over α , β and γ , for Equation 22, are in terms of N and that CFAST uses Equation 14 in terms of \dot{Q} and D , a transformation must be performed. To reach the correct form of the equation, the distributions resulting from the updating process will undergo the same mathematical process as the original values did historically and will be converted to the correct set of parameters. In this conversation process, previously low ranked phenomena become more apparent.

In converting the results obtained updating the joint pdf of the parameters of the empirical Equation 22, new parameters must be considered. Again, in reality the values of g , c_p , ρ , T_0 and fuel specific properties H_c , and r , will not be constants in every different scenario.

As described in section 3.1, in this study, the values for g , c_p , T_∞ , and ρ are kept as constants. The ratio of H_c/r however, is sampled from a uniform distribution. This is done in an attempt to account for the different possible fuel sources. This step was performed in MATLAB.

With distributions now representing those of the correct form of the Equation 14, the model parameters can be sampled multiple times to account for the error resulting from the

historical data used to develop the original equations. Next, distributions over the input values should be considered to account for input uncertainties.

4.3 Input Uncertainties

The only inputs for the flame height sub-model are the HRR of the fire and the base fire diameter. In both the NUREG-1824 reviewed experiments and the NIST experiments uncertainty ranges for the heat release rate are presented. The uncertainties are presented in Table 4-4. In cases for which no uncertainty is reported, expert judgment, given prior experience, should be used to develop the distributions over the heat release rate.

Fire base diameter is also treated with no associated uncertainties. In NUREG-1824 there is a listing of the fuel pool as being a round pan of $1\text{ m} \pm 0.1\text{ m}$ in diameter [3]. However, the source for this listing is that of the report for Benchmark Exercise 4, another experiment set reported in the NUREG-1824. The value of $\pm 0.1\text{ m}$ appears to come from the correct reference for Benchmark Exercise 3 [34], but the uncertainty appears to be in relation to the location of the liquid fuel, and not necessarily an uncertainty in the pan size.

Table 4-4: HRR uncertainties.

Test	\dot{Q} (kW)
BE2	$\pm 15\%$
BE3	$\pm 17\%$
Test 5	$\pm 6\%$
Test 6	$\pm 7\%$
Test 7	$\pm 4\%$
Test 14	$\pm 13\%$
Test 15	$\pm 7\%$
Test 17	$\pm 6\%$
Test 18	$\pm 17\%$
Test 20	$\pm 7\%$
Test 21	$\pm 3\%$

In this thesis an independent source [37] was used to determine a very small measurement uncertainty, representing special dimensions, to develop a distribution over D of ± 0.02 m. Whether or not to include any uncertainty in D will be decided in the initial PIRT. In cases for which the experiment was performed under turbulent conditions the uncertainty in D could become a more influential phenomenon.

With distributions over the inputs and model parameters developed, the sub-model can now be run multiple times using a Monte Carlo simulation resulting in a distribution of the model (code) outputs. As discussed above, the simulations should be run 93 times so as to assure that 95% of the resulting distribution is captured with a 95% confidence as described in the Wilks Tolerance Limit Sampling method.

Using the distributions developed above, to be compared with each different experimental result, 93 random samples of the HRR and D , were run with 93 different samples from the joint distributions of α , β and γ . The result is a 93 x 93 matrix of model predictions for a single test case. These results were ranked in order from smallest to largest, and 93 equally spaced values were taken. The result is the required 93 model predictions necessary to capture the distribution. In the black-box research, a single model prediction was updated with its paired experimental measurement. As discussed above the output updating procedure is slightly more complex.

4.4 Output Updating

To use the black-box model for output updating, an experimental uncertainty for the flame height must be determined. Previously mentioned, the experimental flame heights presented in NUREG-1824 are ranges and not point estimates. In these cases a mid point

over the described range is taken as the experimental result and the uncertainty bounds are described as being within a pan diameter [3]. In the NIST tests, not all the flame heights were presented with experimental uncertainties. In these cases the coefficient of variation was used. Using the data available from other tests, the largest coefficient of variation calculated was used to place an uncertainty on any flame height for which one was not reported. Table 4-5 shows the experimental uncertainties for the flame height.

These uncertainties are taken as the expanded uncertainties (2σ) to be used in the experimental uncertainty analysis as described by NUREG-1824 [3]. Following the process laid out in NUREG-1824, in this analysis the weighted expanded combined experimental uncertainty for use in the black-box model is 13%.

Table 4-5: Flame height expanded uncertainties.

Test	Height (m)
BE2	± 18.6%
BE3	± 17.9%
Test 5*	± 11.1%
Test 6*	± 11.1%
Test 7*	± 11.1%
Test 14	± 9.8%
Test 15	± 8.2%
Test 17	± 8.3%
Test 18	± 11.1%
Test 20	± 8.2%
Test 21	± 10%

**Coefficient of variation used to determine experimental uncertainty*

As stated in section 3.3.2 the complex posterior is currently unsolvable, thus the mean of the model prediction distribution will be compared with the experimental result in the original black-box model. The mean model predictions and experimental results are provided in Table 4-6. Data used in each analysis, including the black-box analysis conducted for comparison, are presented in Appendix B.

Table 4-6: White-box mean model predictions and experimental results.

Mean Model Prediction (m)	Experimental Result (m)
2.0	2.81
3.3	4.3
2.7	2.6
2.4	2.5
3.3	3.5
4.9	5.1
7.1	6.1
6.8	6
4.0	4.5
6.9	6.1
9.8	10

4.5 Overall White-Box Methodology Uncertainty Results

The summary statistics for the marginal posterior marginal pdf's of parameters b_m and s_m are shown in Table 4-7. The distribution of F_m , the multiplicative error factor is also presented in Table 4-7.

Table 4-7: White-box mean summary statistics, Flame height

Parameter	Mean	SD	2.50%	Median	97.50%
b_m	0.032	0.055	-0.077	0.032	0.142
s_m	0.164	0.052	0.090	0.155	0.292
F_m	1.049	0.195	0.718	1.030	1.492

The model uncertainty bounds for the flame height can be determined from the percentiles of F_m . The resulting upper bound is 49%, while the lower bound is -28%. This is shown graphically in Figure 4-5.

Given the value of F_m , it appears that following the white-box analysis, the mean model (code) predictions better match the experimental results compared to the original code predictions. The summary statistics of the standard black-box results are shown in Table 4-8.

The value of F_m for the original model (code) predictions around 0.85 shows that to correct

the model (code) the predictions must be lowered. This suggests a bias in the model to over predict the real flame height.

Compared to the black-box results using the original predictions made by CFAST of 13% and -38% seen in Figure 4-6, using the white-box mean values result in wider uncertainty bounds. This is expected as the white-box approach accounts for the uncertainty inherent in the sub-model.

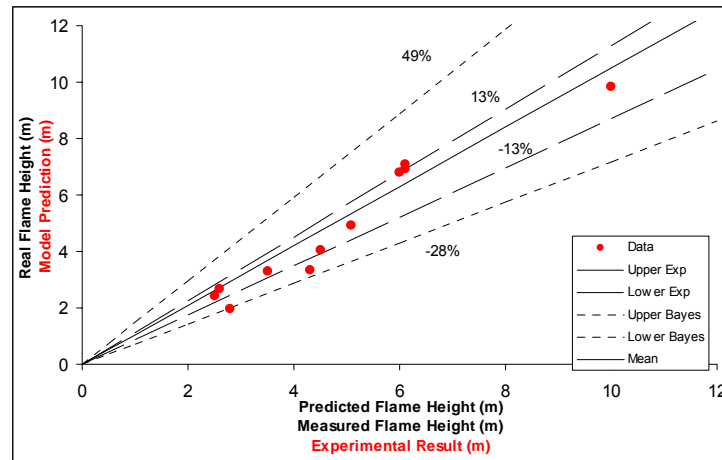


Figure 4-5: White-box mean values used in black-box model flame height results

Table 4-8: Black-box summary statistics, Flame height

Parameter	Mean	SD	2.50%	Median	97.50%
b_m	-0.176	0.0467	-0.268	-0.1761	-0.0835
s_m	0.1337	0.0452	0.0672	0.1265	0.2434
F_m	0.8483	0.1273	0.6246	0.8389	1.133

At first glance, from Figure 4-6 it appears that the uncertainty bounds do not capture the scatter of data. This observation is the consequence of two reasons. First, the scatter of data is assumed to be a result of the error in the experimental results and model (code) predictions. Thus, neither bounds attempt to capture the entire scatter of data alone. Secondly, the results presented for the model (code) uncertainty are those of the model (code)

prediction corrected by the multiplicative error of model to the real value, F_m . Therefore, the bounds presented are those of the model (code) estimation of reality. In cases for which the model (code) has a tendency to over predict the “real” value, as seen in Figure 4-6, the uncertainty bounds will appear to not capture the full scatter of data since the model (code) predictions are greater than the real values. Figure 4-7 explains how to use the results presented.

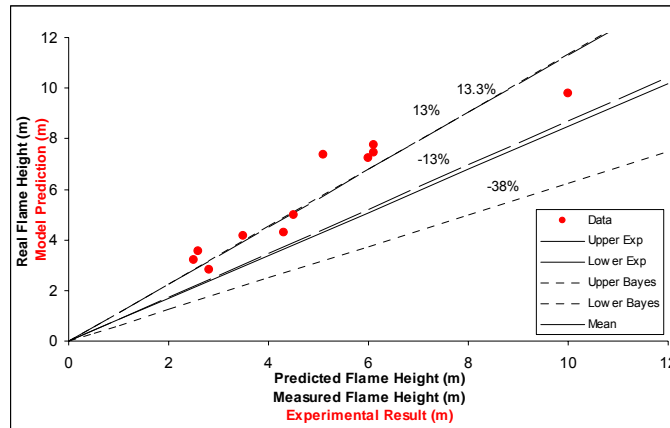


Figure 4-6: Black-box flame height results

In Figure 4-7, a model (code) prediction of the flame height slightly larger than 4 m is assumed. The resulting mean, upper and lower bounds are identified. Observing the data, it appears that CFAST consistently over predicts the flame height when compared to the experimental results. Therefore, the estimation of reality given the model (code) prediction is expected to be lower. In instances where the scatter of data is not as great or there is no clear consistent over or under prediction made by the model (code), the uncertainty bounds will appear to better capture the scatter of data. Such a case is seen in Figure 4-5.

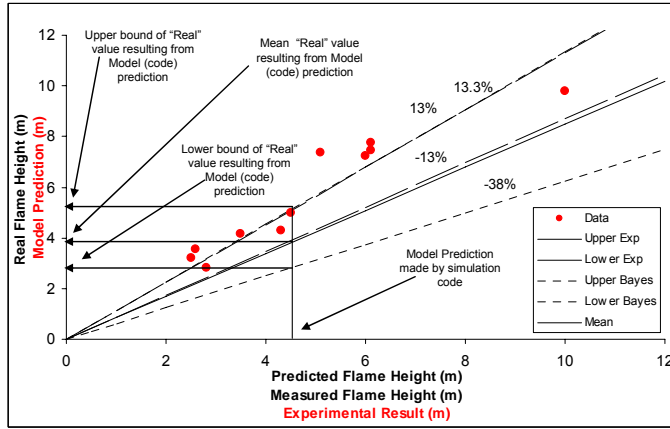


Figure 4-7: Explanation of results

In the second example the sub-model used in CFAST to estimate the plume mass flow will be studied.

Chapter 5: Sub-Model Uncertainty Characterization Example, Plume Mass

Flow in the CFAST Code

The goal of this example will be to show the complexity of propagating the uncertainties throughout the simulation code. The Hot Gas Layer (HGL) is an important fire phenomena often used in fire risk assessment. The HGL temperature can be used to estimate the chance of sprinkler activation or damage to objects in the upper portions of a space such as control cables. In CFAST, the calculation of the HGL temperature is the result of multiple calculations, determined by multiple sub-models. One of these sub-models predicts the mass flow resulting in the fire plume, and thereby the entrainment of air in a fire plume. The routine `mccaffrey.f90` uses equations developed by McCaffrey [38] to determine the mass flow and entrainment of a fire plume. This calculation is broken into three different equations, depending on the region the calculation is being taken in. These regions are determined by the height of the measurement and the HRR. The equations for the flame, intermittent and plume regions are shown below:

$$\text{Flame Region: } \dot{m}_{pl}/\dot{Q}_c = 0.011 \left(z/\dot{Q}_c^{2/5} \right)^{0.566} \quad 0 < \left(z/\dot{Q}_c^{2/5} \right) < 0.08 \quad (25)$$

$$\text{Intermittent Region: } \dot{m}_{pl}/\dot{Q}_c = 0.026 \left(z/\dot{Q}_c^{2/5} \right)^{0.909} \quad 0.08 < \left(z/\dot{Q}_c^{2/5} \right) < 0.2 \quad (26)$$

$$\text{Plume Region: } \dot{m}_{pl}/\dot{Q}_c = 0.124 \left(z/\dot{Q}_c^{2/5} \right)^{1.895} \quad 0.2 < \left(z/\dot{Q}_c^{2/5} \right) \quad (27)$$

where \dot{m}_{pl} is the mass flow in the plume, \dot{Q}_c is the convective HRR, and z is the height

of the measurement. The end result is an estimation of the total plume mass flow at a given height.

5.1 PIRT

A simplified PIRT process with the objective of determining the uncertainty in the plume mass flow sub-model calculations in CFAST is performed. Similar to the flame height example, very few limitations are placed on defining specific scenarios with the goal of not limiting the available data for analysis and increasing the range of application of results. In this example, experimental plume mass flow data will come from tests performed by Zukoski et. al. [39,40] and plume centerline temperature rise and velocity data will be taken from research by McCaffrey [41].

Data for use in estimating the plume mass flow rate were taken from experimental tests performed by Zukoski et al [39]. One objective in the tests performed by Zukoski was to determine the mass of air entrained by a buoyant plume. In these tests the plume mass flow rate is measured under the assumption that the total mass flow rate to the ceiling, \dot{m}_c is a combination of the fuel consumption rate, \dot{m}_f , and the mass of air entrained into the plume, \dot{m}_E . Mass entrained at the interface between the upper HGL and lower cool air, \dot{m}_i and where the plume impinges upon the upper HGL, \dot{m}_p are considered to be negligible.

In these tests two different apparatus were used. In the “far” field, measurements of the plume mass flow rate were taken. The apparatus used for this application is depicted in Figure 5-1.

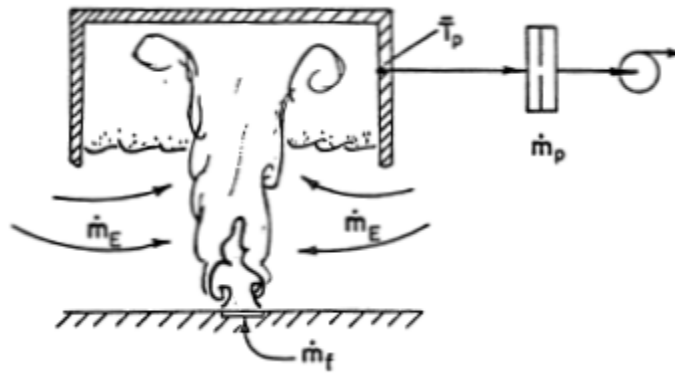


Figure 5-1: Far field plume mass flow rate apparatus [39]

In the “near” field, the method used to determine mass flow rates was to measure the fuel flow rates and the mole fractions of the combustion products in the well-stirred HGL of small hood. From this, the measurement of the concentration of CO_2 or excess O_2 results in a calculation of the overall air-to fuel ratio in the HGL. Therefore, if the amount of fuel supplied is known, the mass of entrained air can be determined. This is different from the far field, since the impingement of the flame into the upper layer results in a non-quietescent layer, weakening the assumption that mass entrained along the boundary layer can be considered negligible. Therefore, the hot gases were allowed to spill out from the smaller hood used to capture the plume. The apparatus can be seen in Figure 5-2.

Plume mass flow rates, for varying source diameters, heat release rates and interface heights were reported by Zukoski [39,40]. Since the plume mass flow is calculated using three different equations used in the simulation code, with respect to the interface height, approximately 15 values for region, flame, intermittent, and plume were taken to be used in this analysis.

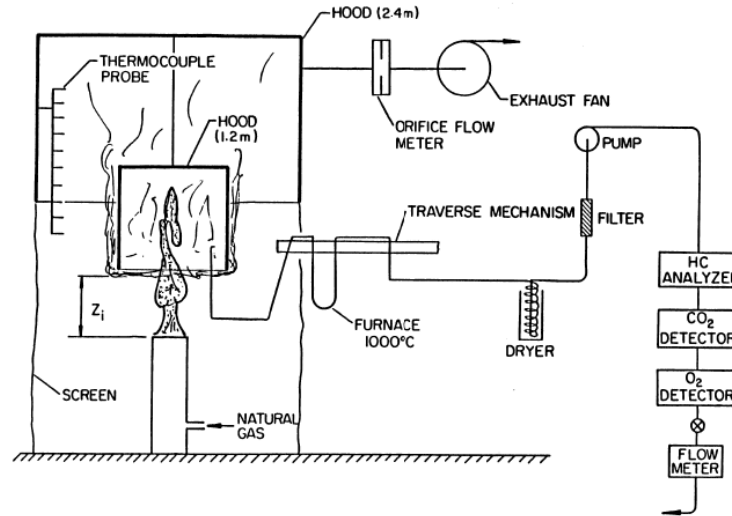


Figure 5-2: Near field plume mass flow rate apparatus [39]

Phenomena and parameters ranked significant are the HRR and the model parameter constants. Similar to the flame height example, the data used in the analysis is not in the form of the final set of equations used in CFAST. Therefore, a number of other parameters and phenomena are identified as the equations are transformed. These parameters, identified later in section 5.2, are determined to rank low enough to be kept as deterministic values.

In CFAST's flame height calculation two non-bookkeeping routines were used. To calculate the plume mass flow CFAST uses three such routines. The routine `mccaffrey.f90` does the main calculation and is therefore ranked high. The `PYROLS.f90` routine again modifies the HRR, and is again ignored. The `mccaffrey.f90` routine is called by another routine, `DOFIRES.f90`. The purpose of this routine in the code is to perform additional modifications of the HRR. One of the modifications made by `DOFIRES.f90` is to limit the HRR to the convective portion only. In this analysis the effects of the `DOFIRES.f90` routine, save the modification of the HRR, are considered low enough to be ignored. To account for the use of the convective HRR in the `mccaffrey.f90` routine the default value of the radiative fraction, 30% [5] used in CFAST is applied to the HRR.

The measurement height z used in this sub-model is the result of a more complex calculation. The plume mass flow is a flow measured at the interface height between the upper and lower layers. This interface is determined by many of the same calculations required to estimate the HGL temperature. These calculations include the movement of mass into and out of the fire compartment through windows, doors, or other openings. The effect of mechanical ventilation could also be considered where applicable. As the goal of this example is not necessarily to report the final estimation of the uncertainty, but to show the application of the proposed method through this example, z will be taken as a constant, given the experimental data.

5.2 Sub-model Parameter Uncertainty

The data used to develop the equations is based on plume centerline temperature and velocity measurements [41]. The measurements are shown Figure 5-3 a, b.

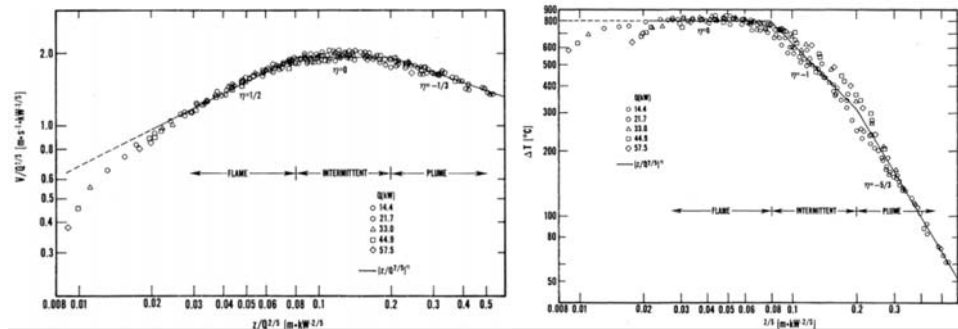


Figure 5-3: Plume Centerline Velocity (a) and Temperature Rise (b) [41]

Using the data presented in Figure 5-3, equations for the centerline velocity and temperature rise were developed by McCaffrey [41]:

$$U(z)/\dot{Q}_c^{1/5} = A_n \left(z/\dot{Q}_c^{2/5} \right)^n \quad (28)$$

$$a(z) = \Delta T(z)/T_\infty = (B_n/T_\infty) \left(z/\dot{Q}_c^{2/5} \right)^{2n-1} \quad (29)$$

where U is the centerline velocity, A_n is the coefficient of centerline velocity variation, n is the exponent of centerline velocity and temperature rise variation with height, a is the normalized centerline temperature rise variation, and B_n is the coefficient of centerline temperature rise.

McCaffrey recognized these relations could be used to estimate the mass flow in a plume. Assuming axial symmetry, McCaffrey estimated that the mass flow rate at any height could be estimated using [41]:

$$m(z) = \int_0^\infty \bar{\rho} \bar{u}(z, x) 2\pi x dx \quad (30)$$

The relation between ρ and u , the flow velocity, was not well understood, leading McCaffrey to use his relations for centerline velocity and temperature rise. He also assumed a single characteristic width of $x_{1/e}$ for both the velocity and temperature rise. The result is an estimated mass flow relation:

$$m(z) = \pi \rho_\infty (x_{1/e})^2 \frac{U(z)}{\Delta T(z)/T_\infty} \ln \left(\frac{\Delta T(z)}{T_\infty} + 1 \right) \quad (31)$$

which, using the experimental values of centerline velocity and temperature rise, results in the following simplified expression of the mass flow in the near field:

$$\dot{m} = 0.055 z \dot{Q}^{1/2} \quad (32)$$

This is the first relation of McCaffrey presents for the estimation of the mass flow rate. It is slightly different than the comparable equation used in CFAST, Equation 25. Two papers and four years later McCaffrey would present a more robust calculation of the mass flow rate. A major difference between McCaffrey's original mass flow analysis and the final

analysis performed years later is the assumption of a single characteristic profile for both the velocity and temperature rise. He would however continue to use his original relations for the centerline velocity and temperature rise.

The result is a relation for the total mass flow rate given the following equations [38]:

$$m(z) = \pi\rho_\infty [\sigma_v(z)]^2 \cdot U(z) \cdot I_\lambda(a) \quad (33)$$

with,

$$\sigma_v(z) = \frac{C_\lambda [I_\lambda(a)]^{\lambda^2/4C_B}}{[U(z) \cdot \sqrt{K_\lambda(a)}]} \quad (34)$$

where m is the total mass flow rate, σ_v is the $1/e$ width of radial profile, λ is the ratio of thermal to velocity profiles, C_B is the local buoyancy constant, and I_λ and K_λ are analytical functions of a .

Distributions over the equation parameters A_n and B_n were developed using the historical data in Figure 5-3. Once again an empirical form of Equations 28 and 29 are developed and used in a Bayesian framework.

$$U(z) = \alpha \left(\frac{z}{\dot{Q}_c^{2/5}} \right)^n \dot{Q}_c^{1/5}, \quad a(z) = \frac{\beta}{T_\infty} \left(\frac{z}{\dot{Q}_c^{2/5}} \right)^{2n-1} \quad (35,36)$$

In Equations 35 and 36, the values of n are dependent upon which zone the estimation is being made in. For this reason, no distribution was developed for the values of n , and it was kept as a constant that changed with a change in the zone in which the measurement was being taken. The resulting posterior for the centerline velocity equation is:

$$f(\alpha | U, z, Q) = \frac{f_0(\alpha) \times L(U, z, Q | \alpha)}{\int_{\alpha} f_0(\alpha) \times L(U, z, Q | \alpha) d\alpha} \quad (37)$$

where:

$$L(U, z, \dot{Q}_c | \alpha) = \prod_{i=1}^n \frac{1}{\sqrt{2\pi}\sigma} e^{-\frac{1}{2\sigma^2} \left[\frac{U - \alpha \left(\frac{z}{\dot{Q}_c^{2/5}} \right)^n \dot{Q}_c^{1/5}}{\sigma} \right]^2} \quad (38)$$

with $f_0(\alpha)$, prior distribution of parameter α , and $f(\alpha | U, z, \dot{Q}_c)$, posterior distribution of parameter α . A similar framework and likelihood is developed for the centerline temperature data. Distributions over A_n and B_n are developed in each zone.

These pdf's of the sub-model parameters are sampled and used in Equations 33 and 34 following the steps laid out by McCaffrey in his development of the historical equations. Just as in the flame height example, new phenomena are identified in following these steps. New phenomena include π , c_p , ρ , T_{∞} , and other constants C_B , λ and C_{λ} . In this work, the uncertainty importance of each phenomenon was decided to be small enough to be kept as constants. However, similar to the results of the sensitivity analysis performed in the flame height example, under a more robust application of this methodology, ignoring the variation in the excluded phenomena may not be the best assumption.

Having applied the distributions over A_n and B_n to Equations 28 and 29 of which the results were used in Equations 33 and 34, multiple estimations of the total mass flow are made. These results were used to update the parameters in the equations used in CFAST. Empirical equations are developed again and used in a Bayesian framework.

$$\dot{m}_{pl} / \dot{Q}_c = \alpha \left(\frac{z}{\dot{Q}_c^{2/5}} \right)^{\beta} \quad (39)$$

The resulting posterior is shown in 39.

$$f(\alpha, \beta | z, \dot{Q}_c) = \frac{f_0(\alpha, \beta) \times L(z, \dot{Q}_c | \alpha, \beta)}{\iint_{\alpha \beta} f_0(\alpha, \beta) \times L(z, \dot{Q}_c | \alpha, \beta) d\alpha d\beta} \quad (40)$$

where:

$$L(z, \dot{Q}_c | \alpha, \beta) = \prod_{i=1}^n \frac{1}{\sqrt{2\pi}\sigma} e^{-\frac{1}{2} \times \frac{\left[\frac{m/\dot{Q}_c - \alpha \left(\frac{z}{\dot{Q}_c^{2/5}} \right)^\beta \right]^2}{\sigma}} \quad (41)$$

with $f_0(\alpha, \beta)$, prior joint distribution of parameters and $f(\alpha, \beta | z, \dot{Q}_c)$, posterior joint distribution of parameters.

This step is carried out for each region of the fire plume. The resulting distributions will be sampled from and used in the mcaffrey.f90 routine similar to the steps described in the flame height example.

One difference between this example and the flame height example is that the calculation performed in CFAST is not exactly the same as that shown in the literature. In CFAST to ensure the mass flow is continuous between regions, the values of what would be α in the empirical equations for the intermittent and plume regions, are calculated in the following manner [5]:

$$\alpha_I = \alpha_F \left(\frac{z}{\dot{Q}_c^{2/5}} \right)^{\beta_F} / \left(\frac{z}{\dot{Q}_c^{2/5}} \right)^{\beta_I} \quad \text{for a } \frac{z}{\dot{Q}_c^{2/5}} \text{ of } 0.08 \quad (42)$$

and,

$$\alpha_P = \alpha_I \left(\frac{z}{\dot{Q}_c^{2/5}} \right)^{\beta_I} / \left(\frac{z}{\dot{Q}_c^{2/5}} \right)^{\beta_P} \quad \text{for a } \frac{z}{\dot{Q}_c^{2/5}} \text{ of } 0.2 \quad (43)$$

where the subscript F refers to the flame region, I refers to the intermittent region and P refers to the plume region.

Due to this representation, the marginal distributions of α and β as determined by the Bayesian inference, will be separated. This results in an additional source of uncertainty being introduced as the values of α and β are no longer being paired and could be combined such that a large estimation of α is paired with a small estimation of β .

There are two special notes that should be pointed out at this stage of the analysis. First, the author was unable to reach results similar to those reported by McCaffrey for the flaming region. As a result, the coefficient of variation was once again used to develop distributions over the values of α_F . The values of β_I and β_P used were those developed in the Bayesian framework. However, the values of α_I and α_P are determined by Equations 42 and 43, and thus are directly related to the estimated value of α_F .

Secondly, as a result of the necessary simulations, an attempt was made to modify the original FORTRAN code to accept and report multiple values, similar to steps taken in the flame height example. Unfortunately, this modification was not completed and the results were calculated in MATLAB. These results were compared to single point estimations made by the FORTRAN code and confirmed to be correct within four to five decimal places. The MATLAB code used in the analysis is provided in Appendix C.

5.3 Input Uncertainties

The only input taken to be uncertain in this example is the convective HRR since the interface height, z , is taken to be constant. No direct mention of the uncertainty over the

value of \dot{Q}_c in the experiments is discussed in the reports listing the data [39,40]. An uncertainty in \dot{Q}_c of 25% was used in this study in an attempt to be conservative.

5.4 Output Updating

Again, using the likelihood from the black-box analysis, an estimation of the experimental uncertainty must be determined. Similar to the information available about uncertainty in the HRR, there is no discussion of any uncertainty in the experimental results in the reports [39,40]. There is however, discussion of the devices used to measure the CO₂, CO, O₂ and un-burnt hydrocarbons [39]. Taking a quick look at other reports, it appears that when calibrated, the uncertainty in the measurements made by the devices listed in the experimental tests reports [39,40] can be as low as $\pm 1-2\%$ [42,43]. Pairing this knowledge with the description that the plume mass flow was determined by measuring the fuel flow rates and combustion products mole fractions, a subjective experimental uncertainty of 15% is used in this analysis. This number is kept low in attempt to not over attribute the scatter of data to the experimental results.

Comparing equations developed by different researchers [44] shown in Table 5-1, except for those developed by McCaffrey which was done following a more theoretical approach, each equation is very similar to the others. Using this observation, it is not expected that the measurement uncertainty would be very large since it appears each researcher was arriving at similar results.

Table 5-1: Plume mass flow rate equations [44]

Researcher	Equation
McCaffrey	$\dot{m}_{pl} = 0.124 \left(z / \dot{Q}_c^{2/5} \right)^{1.895} \cdot \dot{Q}_c$
Zukoski	$\dot{m}_{pl} = 0.076 \left(z / \dot{Q}_c^{2/5} \right)^{5/3} \cdot \dot{Q}_c$
Ricou and Spalding	$\dot{m}_{pl} = 0.066 \left(z / \dot{Q}_c^{2/5} \right)^{5/3} \cdot \dot{Q}_c$
Yokoi	$\dot{m}_{pl} = 0.076 \left(z / \dot{Q}_c^{2/5} \right)^{5/3} \cdot \dot{Q}_c$
Heskestad	$\dot{m}_{pl} = 0.071 \left(z / \dot{Q}_c^{2/5} \right)^{5/3} \cdot \dot{Q}_c$
Cox and Chitty	$\dot{m}_{pl} = 0.082 \left(z / \dot{Q}_c^{2/5} \right)^{5/3} \cdot \dot{Q}_c$

5.5 White-Box Uncertainty Results

Using the white-box analysis mean value of the distributions of predictions by the simulation code compared to the experimental results, the summary statistics for each region are shown in Tables 5-2, 5-3 and 5-4.

Table 5-2: Flame Region Summary Statistics using white-box mean

Parameter	Mean	SD	2.50%	median	97.50%
b_m	0.5069	0.5491	-0.5805	0.5024	1.604
s_m	2.052	0.4353	1.403	1.983	3.109
F_m	24.85	333.4	0.0249	1.661	120.7

Table 5-3: Intermittent Region Summary Statistics using white-box mean

Parameter	Mean	SD	2.50%	median	97.50%
b_m	-0.4282	0.1206	-0.6698	-0.4272	-0.1869
s_m	0.4508	0.0982	0.3035	0.4355	0.6844
F_m	0.7342	0.3985	0.2575	0.6502	1.743

Table 5-4: Plume Region Summary Statistics using white-box mean

Parameter	Mean	SD	2.50%	median	97.50%
b_m	-0.0281	0.0592	-0.1455	-0.0278	0.0905
s_m	0.2118	0.0522	0.1332	0.2041	0.333
F_m	0.9974	0.2295	0.6214	0.9741	1.525

Looking at the value of F_m in Table 5-2 for the flame region and Figure 5-4 it is clear that CFAST does a poor job predicting the plume mass flow in the flame region. The resulting model uncertainty bounds are 11970% to -97.5%. This does not appear to be a result of the white-box analysis as similar wide bounds are observed upon performing the black-box analysis using the original estimations made by CFAST seen in Figure 5-5.

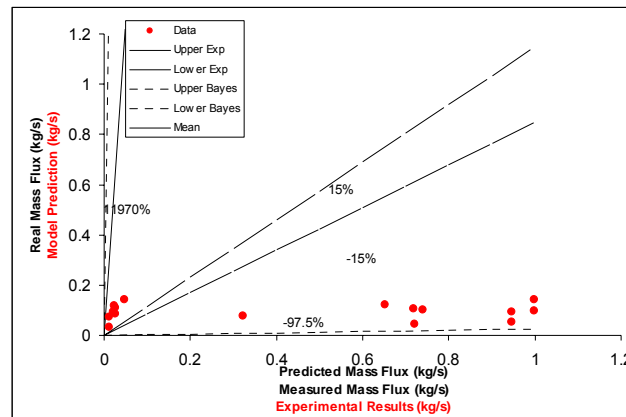


Figure 5-4: White-box mean results in black-box model, Flame region, Plume mass flow rate

In the report of the experiments by Zukoski, it is stated that in the near (flame region) field, the results do not appear to be a strong function of the HHR, but are instead influenced by the fuel diameter [39]. Since, McCaffrey's equation does not consider the diameters at all, but calculates results as a function of interface height z and HRR, the result of this analysis could be used to show a weakness in using McCaffrey's equation in the flame region. This observation is an added bonus to performing the white-box analysis of a sub-model. Not only

are the uncertainties in the sub-model determined, but as a result of peering deep into the relations used within the simulation codes, instances in which the model (code) does a particularly poor job can be observed. This result could be more significant following a more complex analysis involving multiple sub-models for which a large uncertainty will not want to be carried through the calculation.

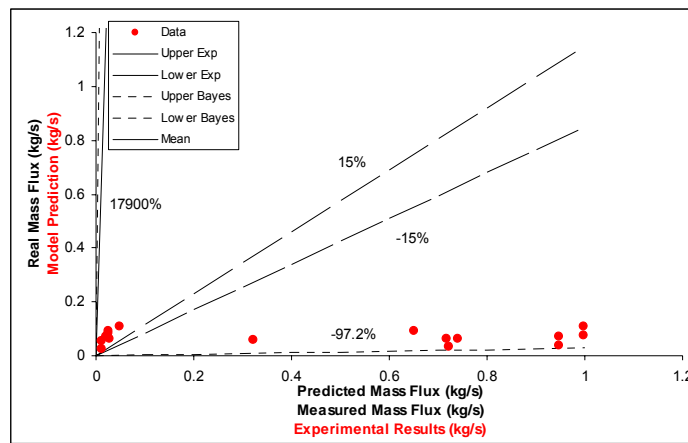


Figure 5-5: Black-box flame region plume mass flow rate results

The model (code) uncertainty bounds following the white-box analysis for the plume region are 74.3% and -74.3% presented graphically in Figure 5-6, while the bounds are 52.5% and -37.9% for the black-box estimate of the plume region as shown in Figure 5-7.

Similar to the results seen in the flame height example, comparing the results presented in Tables 5-2, 5-3 and 5-4 to those of the black-box analysis shown in Tables 5-5, 5-6 and 5-7 using the original CFAST predictions, the white-box approach results in larger uncertainty bounds. Just as in the flame height example, these wider bounds are a result of the white-box analysis accounting for additional uncertainties in the input and sub-model parameters.

Table 5-5: Black-box flame region plume mass flow summary statistics

Parameter	Mean	SD	2.50%	median	97.50%
b_m	0.8176	0.5542	-0.2793	0.8189	1.924
s_m	2.092	0.451	1.424	2.021	3.175
F_m	59.35	2480	0.0281	2.269	180

Table 5-6: Black-box intermittent region plume mass flow summary statistics

Parameter	Mean	SD	2.50%	median	97.50%
b_m	-0.4692	0.1209	-0.709	-0.4692	-0.2302
s_m	0.4484	0.0979	0.301	0.433	0.6773
F_m	0.7016	0.3743	0.2432	0.6226	1.627

Table 5-7: Black-box plume region plume mass flow summary statistics

Parameter	Mean	SD	2.50%	median	97.50%
b_m	-0.3486	0.0527	-0.451	-0.3489	-0.2443
s_m	0.1842	0.0458	0.1135	0.1776	0.291
F_m	0.7201	0.1429	0.4786	0.7065	1.042

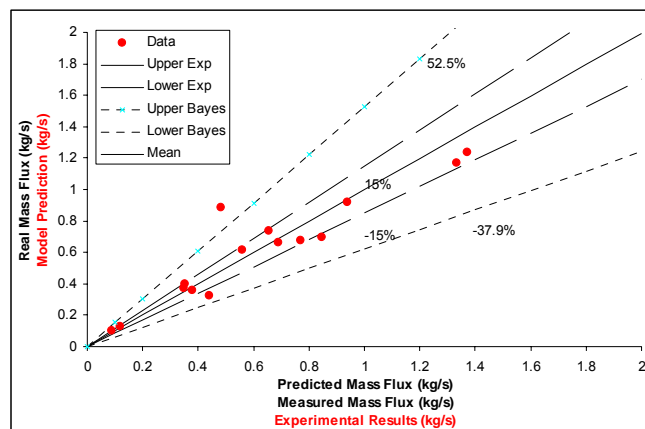


Figure 5-6: White-box mean results in black-box model, Plume region, Plume mass flow rate

Looking at the original data in the plume region (Figure 5-7), it appears the model (code) continuously over predicted the plume mass flow. This observation is also seen in the multiplicative error fraction, F_m , of 0.72. Since F_m is used to correct the model prediction to

an estimation of the real value, an F_m lower than 1 means that the model (code) prediction must be lowered to estimate the real value.

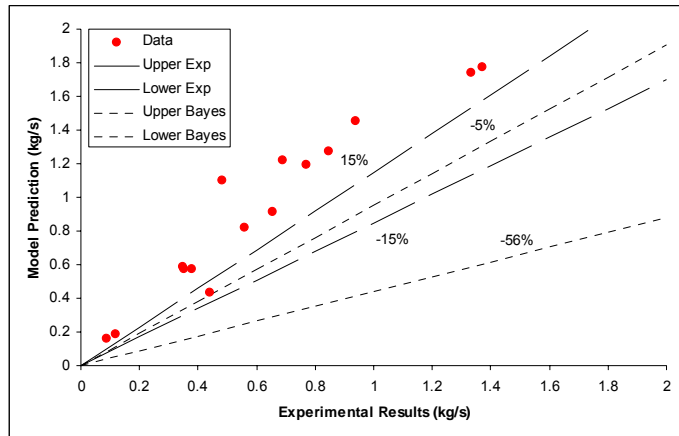


Figure 5-7: Black-box model results, Plume region, Plume mass flow rate

In the results of the white-box analysis (Figure 5-6), this is not the case. Taking a quick glance at the data, the model (code) predictions are no longer seen to be constant over-predicting the experimental measurements. The scatter of the data also appears to be somewhat larger. These observations are strengthened given the results estimation of F_m . F_m value from the white-box is much closer to 1 with a value of 0.9974. The standard deviation has also grown from a value of 0.1429 for the original CFAST predictions to a value of 0.2295 for the white-box mean value predictions. This is very similar to the observations made in the flame height analysis, where it appeared that in accounting for the uncertainty in the inputs and the sub-model parameters resulted in a less bias prediction being made by the model (code).

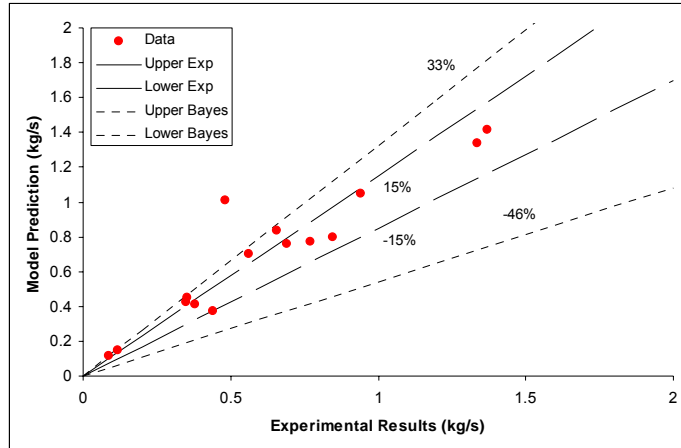


Figure 5-8: Black-box intermittent region plume mass flow rate results

Similar observations can be made comparing the results in the intermittent region. While not as pronounced as in the plume region, the intermittent region results following the white-box analysis are, slightly, closer to those of the experiment seen comparing the value of F_m in Tables 5-3 and 5-6.

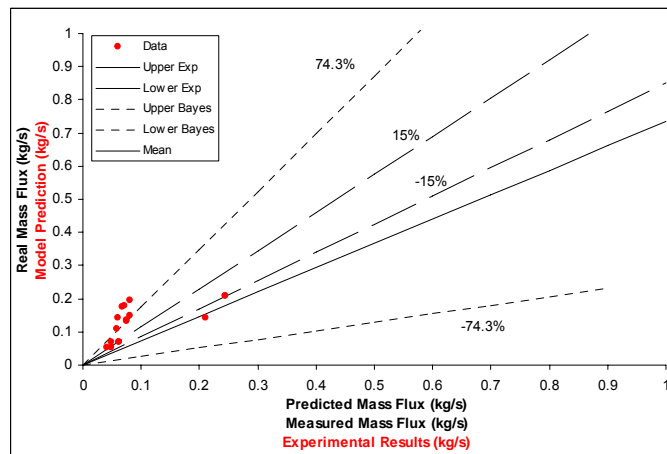


Figure 5-9: White-box mean values used in black-box model, Intermittent region, Plume mass flow rate

The change in the model (code) bias following the white-box analysis can be seen in either a positive or negative light. Positively, following the white-box approach, the

predictions made by the model (code) are closer to the expected values measured in experiments. This could be lightly thought of as that the code doing a better job predicting the real value.

Taking the other view point, with out following the white-box approach, the model (code) appears to constantly over predict reality. With this knowledge, the results of the model (code) prediction can be taken as a conservative estimate of damage resulting from a flame impingement risk analysis point of view (for detection purposes this may not be the case as estimated flame heights may suggest a larger, more visible flame height where one will not be observed.) This same judgment can not be made given the results following the white-box approach. The white-box results, in matching better with the experimental measurements, can not be considered to be a conservative estimate. Better estimating the results with no clear bias means that the white-box predictions could be higher or lower than the real value.

The objective of this analysis as stated in the beginning was to determine an estimation of the uncertainty in the model prediction of the plume mass flow calculation by CFAST and introduce the complexity of the propagation of uncertainty from the plume mass flow calculation to the HGL temperature estimation.

5.6 Propagation of Results

For use in the uncertainty analysis of the HGL temperature calculation by CFAST the plume mass flux results must be propagated through the code structure. The source code for CFAST can be found online at <http://cfast.nist.gov/> [45].

Following the code structure, the results of the plume mass flux calculation performed by the routine `mccaffrey.f90` are eventually used in the routine `RESID.f90` to calculate the HGL temperature. This simple code structure is shown in Figure 5-10.

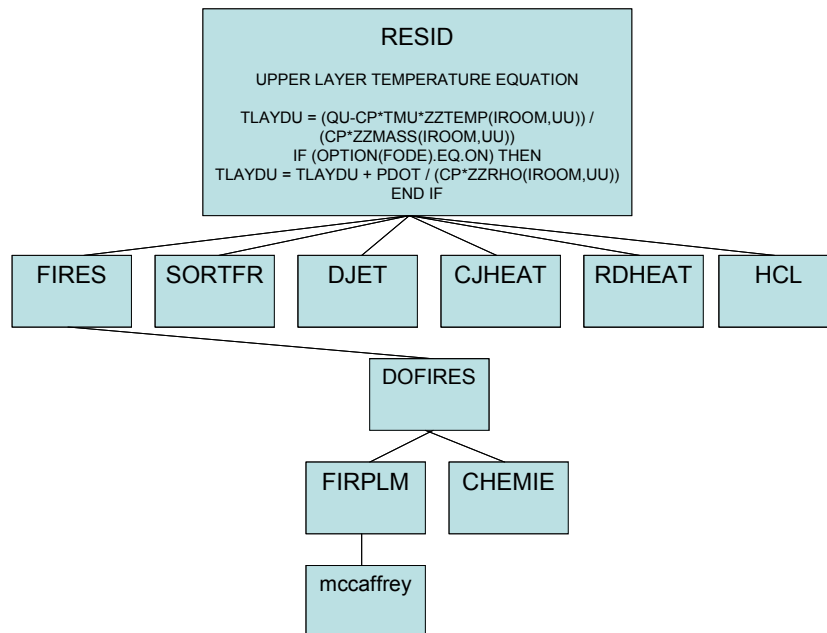


Figure 5-10: Code Structure, plume mass flow rate to HGL temperature calculation

In Figure 5-10 only the path of the plume mass flux results with respect to the HGL temperature calculation are shown. The HGL temperature is also a function of many other calculations. `RESID` calculates the HGL temperature using the flow of energy and mass as reported in calculations of multiple other routines.

The results calculated by `mccaffrey.f90` are the plume mass flux, `XEMS` and the plume mass entrainment, `XEME`. These results are called by the routine `FIRPLM.f90`. This routine is merely a “bookkeeping” routine and does not modify the results calculated by `mccaffrey.f90`. `FIRPLM.f90` is in turn called by a routine `DOFIRES.f90`.

In DOFIRES.f90 the plume mass flux and entrainment results are modified by another routine, CHEMIE.f90. CHEMIE.f90 accounts for the oxygen available for combustion. In performing the full HGL layer uncertainty analysis the uncertainty within the CHEMIE.f90 routine may need to be considered. If there is no limit to the available oxygen, the CHEMIE.f90 routine could be ignored in the HGL temperature analysis.

The next routine in line is FIRES.f90. In FIRES.f90 the values of XEMS and XEME are transformed into the flow of energy and mass. The FIRES.f90 routine transformation of XEMS and XEME to flows of mass and energy would need to undergo uncertainty analysis in the full estimation of uncertainty in the HGL temperature calculation.

Figure 5-10 shows that FIRES.f90 is called by RESID.f90. Here the flow of energy and mass of the fire is combined with the flows of energy and mass calculated elsewhere in the program. Other flows are those resulting from doors, radiation, or other fires. These flows are combined into total flows of mass and energy. The term “QU” in Figure 5-10 is the total energy flow in the upper layer and “TMU” is the total mass flow in the upper layer used to calculate the HGL temperature.

It is clear from this quick review of the code structure that the HGL temperature uncertainty analysis would be extremely involved and time consuming. Not discussed directly in the explanation above is the estimation of the layer height interface z . The layer height will be calculated given the layer volume calculation also performed in RESID.f90. Also, the uncertainty analysis for the flows calculated in the routines DJET.f90, CJHEAT.f90, RDHEAT.f90, etc. would need to be considered in the full HGL temperature uncertainty analysis.

Chapter 6: Conclusions

This methodology presents a systematic process to account for uncertainties in fire simulation codes. The uncertainties resulting from inputs and sub-model parameters are considered and propagated through the simulation code following the Wilks Tolerance Limit sampling technique. The resulting model (code) predictions are updated with experimental measurements resulting in a characterization of the uncertainty resulting in a model (code) prediction.

In the two examples presented, the uncertainty bounds for the white-box analysis were wider than those of a black-box analysis. The larger bounds are a result of the recognition, quantification and inclusion of input and parameter uncertainties associated with sub-models. Also seen in the two examples, despite an increase in scatter, the modification of the model (code) predictions as a result of the white-box analysis appears to have lessened the bias of the model (code) predictions. In both examples, the original model (code) predictions were consistently larger than the results of experiments. After accounting for the input and parameter uncertainties, the model (code) predictions, despite wider over all bounds, appear to have lost most of their bias.

As shown in the plume mass flow example, an added advantage of applying this methodology is observing the weaknesses of poor sub-model calculations. These observations can be used to show where future research focus is needed or where the choice to use other sub-models should be made.

Applying the proposed methodology involves complex Bayesian posterior calculations and the general effort required to apply the methodology. Solution of non-paired data as discussed earlier requires further research to offer a more robust and complete

numerical solution. To apply this methodology to a complex calculation encompassing multiple sub-models would require not only an advanced knowledge of fire phenomena, but an in-depth knowledge of the simulation code structure and language. By choosing to shoulder the difficulty of taking the time to develop a complete understanding of the code calculation and undertake the complex posterior calculation, allows for a more complete representation of the model (code) uncertainty.

6.1 Future Research

The results presented in this work outline a methodology for determining the uncertainty within a fire simulation code. The methodology has been shown using two simple examples. The following suggestions are made with respect to future research which may advance the ability to apply this methodology using fewer assumptions on current and future fire simulation models.

- The Bayesian inference used in the examples presented are of the simple black-box approach. The author is not currently aware of a computer program capable of solving the complex inference presented for the white-box analysis. Creating a program, or modifying a current program to solve this inference would greatly reduce the approximations inherent in choosing to use the black-box inference.
- Not addressed in this work is the issue to presenting the results following the white-box analysis. Should this analysis ever be applied to an entire code, presenting the results would be a very difficult task.
- This methodology was presented by example using the simulation code CFAST. It is expected that this methodology can be used on other fire simulation codes including

FDT's, FIVE-Rev1, and MAGIC (assuming the code structure and sub-models used are similar to that of CFAST.) The author has not studied the code structure of the simulation code FDS. FDS is one of the most popular fire simulation models in use today. While, the overall methodology is expected to be applicable, the application is expected to be more involved and time consuming resulting from the differences in the code structure and calculations made by FDS. Therefore, the author suggests that the FDS code structure and sub-models used be reviewed with an eye for applying this methodology.

Appendices

Appendix A: Summary Statistics

White-Box

Table A-1: Black-box/White-box summary statistics, Flame height

Model Uncertainty - Flame Height		CFAST
Parameter		
Black-Box	μ	-0.1765
	σ	0.1493
White-Box	μ	0.03091
	σ	0.1813

Table A-2: Black-box/White-box summary statistics, Plume mass flow

Model Uncertainty - Plume Mass Flow		CFAST
Parameter		
Black-Box Flame Region	μ	0.8167
	σ	2.206
Black-Box Intermittent Region	μ	-0.4704
	σ	0.4779
Black-Box Plume Region	μ	-0.3474
	σ	0.1949
White-Box Flame Region	μ	0.5112
	σ	2.143
White-Box Intermittent Region	μ	-0.4254
	σ	0.4765
White-Box Plume Region	μ	-0.02809
	σ	0.2258

Appendix B – Data

Table B-1: Black-box model predictions and experimental results.

Model	Experimental
Prediction (m)	Result (m)
2.8	2.81
4.3	4.3
3.6	2.6
3.2	2.5
4.2	3.5
7.4	5.1
7.8	6.1
7.3	6.0
5.0	4.5
7.4	6.1
9.8	10.0

Table B-2: White-box mean model predictions and experimental results.

Mean Model	Experimental
Prediction (m)	Result (m)
2.0	2.81
3.3	4.3
2.7	2.6
2.4	2.5
3.3	3.5
4.9	5.1
7.1	6.1
6.8	6.0
4.0	4.5
6.9	6.1
9.8	10.0

Table B-3: Black-box model predictions and experimental results, flame region.

Model	Experimental
Prediction (kg/s)	Result (kg/s)
0.0562	0.0126
0.0593	0.3226
0.0704	0.0202
0.0240	0.0121
0.0832	0.0258
0.0904	0.0242
0.0924	0.6514
0.0642	0.0267
0.0350	0.7207
0.0721	0.9462
0.0732	0.9973
0.1102	0.0479
0.0368	0.9474
0.0625	0.7410
0.0625	0.7184

Table B-4: Black-box model predictions and experimental results, intermittent region.

Model	Experimental
Prediction (kg/s)	Result (kg/s)
0.1443	0.0598
0.0531	0.0421
0.1115	0.0579
0.1835	0.0686
0.1865	0.0719
0.2026	0.0800
0.1373	0.0749
0.1416	0.0749
0.0718	0.0493
0.0746	0.0614
0.1490	0.2105
0.1565	0.0809
0.2199	0.2450
0.0531	0.0493
0.0720	0.0615

Table B-5: Black-box model predictions and experimental results, plume region.

Model	Experimental
Prediction (kg/s)	Result (kg/s)
1.0079	0.4820
0.8389	0.6560
0.7497	0.5600
0.3988	0.4390
1.6292	1.3700
0.1716	0.1170
0.5250	0.3540
1.5936	1.3340
0.1451	0.0890
0.5362	0.3480
1.3309	0.9400
0.5241	0.3790
1.0944	0.7690
1.1680	0.8450
1.1189	0.6900

Table B-6: White-box mean model predictions and experimental results, flume region.

Mean Model	Experimental
Prediction (kg/s)	Result (kg/s)
0.0737	0.0126
0.0777	0.3226
0.0922	0.0202
0.0314	0.0121
0.1090	0.0258
0.1184	0.0242
0.1210	0.6514
0.0842	0.0267
0.0456	0.7207
0.0945	0.9462
0.0961	0.9973
0.1443	0.0479
0.0510	0.9474
0.1037	0.7410
0.1058	0.7184

Table B-7: White-box mean model predictions and experimental results, intermittent region.

Mean Model Prediction (kg/s)	Experimental Result (kg/s)
0.1413	0.0598
0.0515	0.0421
0.1083	0.0579
0.1769	0.0686
0.1796	0.0719
0.1940	0.0800
0.1315	0.0749
0.1354	0.0749
0.0683	0.0493
0.0707	0.0614
0.1421	0.2105
0.1486	0.0809
0.2090	0.2450
0.0515	0.0493
0.0685	0.0615

Table B-8: White-box mean model predictions and experimental results, plume region.

Mean Model Prediction (kg/s)	Experimental Result (kg/s)
0.8826	0.4820
0.7342	0.6560
0.6149	0.5600
0.3268	0.4390
1.2371	1.3700
0.1303	0.1170
0.3964	0.3540
1.1701	1.3340
0.1001	0.0890
0.3712	0.3480
0.9178	0.9400
0.3585	0.3790
0.6759	0.7690
0.6987	0.8450
0.6624	0.6900

Appendix C: Computer Codes

WinBUGS Files:

Empirical flame height parameter estimation:

```
model {
  a~dunif(-3,3)
  b~dunif(0,20)
  g~dunif(0,1)
  s~dunif(0,1)

  C <- 1000

  for( i in 1 : N ) {
    zeros[i] <- 0
    L[i] <- exp(-0.5*pow((x[i,2]-a-
b*pow(x[i,1],g))/s,2))/(pow((2*3.141592654),0.5)*s)
    ghr[i] <- ( -1 ) * log(L[i]) + C
    zeros[i] ~ dpois(ghr[i])
  }
  tau<-1/pow(s,2)
  e~dnorm(0,tau)

  for (j in 1:10){
    y0[j]<-a+b*pow(x0[j],g)+e
  }
}
```

Modified CFAST FORTRAN code fheight.f90

```
!23456789012345678901234567890123456789012345678901234567890123456789012
```

```
PROGRAM test
IMPLICIT NONE
real*8, parameter :: zero = 0.0d0, four = 4.0d0, pi = 3.14159d0
INTEGER, PARAMETER :: Numtimes = 291
REAL, DIMENSION(Numtimes,1) :: a=0, b=0, c=0, qdot=0, area=0
REAL, DIMENSION(Numtimes,Numtimes) :: fheight=0
integer i,j, OpenStatus, InputStatus, k, g
real, DIMENSION(Numtimes,1) :: d=0

OPEN(UNIT=10,FILE="area.dat",STATUS="OLD", IOSTAT = OpenStatus)
IF (OpenStatus > 0) STOP "**** Cannot open the file****"
OPEN(UNIT=11,FILE="qdot.dat",STATUS="OLD", IOSTAT = OpenStatus)
IF (OpenStatus > 0) STOP "**** Cannot open the file****"
OPEN(UNIT=12,FILE="a.dat",STATUS="OLD", IOSTAT = OpenStatus)
IF (OpenStatus > 0) STOP "**** Cannot open the file****"
OPEN(UNIT=13,FILE="b.dat",STATUS="OLD", IOSTAT = OpenStatus)
IF (OpenStatus > 0) STOP "**** Cannot open the file****"
OPEN(UNIT=14,FILE="c.dat",STATUS="OLD", IOSTAT = OpenStatus)
IF (OpenStatus > 0) STOP "**** Cannot open the file****"

DO i=1,Numtimes
  READ(10,*, IOSTAT = InputStatus) area(i,1)
  IF ( InputStatus > 0 ) STOP "****Input error****"
  IF ( InputStatus < 0 ) EXIT ! end of file
  READ(11,*, IOSTAT = InputStatus) qdot(i,1)
  IF ( InputStatus > 0 ) STOP "****Input error****"
  IF ( InputStatus < 0 ) EXIT ! end of file
  READ(12,*, IOSTAT = InputStatus) a(i,1)
  IF ( InputStatus > 0 ) STOP "****Input error****"
  IF ( InputStatus < 0 ) EXIT ! end of file
  READ(13,*, IOSTAT = InputStatus) b(i,1)
  IF ( InputStatus > 0 ) STOP "****Input error****"
  IF ( InputStatus < 0 ) EXIT ! end of file
  READ(14,*, IOSTAT = InputStatus) c(i,1)
  IF ( InputStatus > 0 ) STOP "****Input error****"
  IF ( InputStatus < 0 ) EXIT ! end of file
END DO

DO k=1,Numtimes
  DO j=1,Numtimes
    if (area(j,1).le.0d0) THEN
      d = 0.3d0
    else
      d(j,1) = SQRT(four*area(j,1)/pi)
    end if
    fheight(j,k) = a(k,1)*d(j,1) + b(k,1)*(qdot(j,1)/1.0d0)**c(k,1)
    fheight(j,k) = max (zero, fheight(j,k))
  END DO
END DO
OPEN(15, FILE='fheight20-93.csv')
DO g=1, Numtimes
```

```
WRITE(15,100) fheight(g,1:291)
END DO
100 FORMAT(397E13.6)

CLOSE (10)
CLOSE (11)
CLOSE (12)
CLOSE (13)
CLOSE (14)
END PROGRAM test
```

Flame Height Output Updating Model:

```
+model;
{
  bm~dunif(-5,5)
  sm~ dunif(0,5)
  taum<-1/pow(sm,2)
  pe<-0.13

  be<-(log(1+pe)+log(1-pe))/2
  se<-(log(1+pe)-log(1-pe))/(2*1.95996398454005)

  bt<-bm-be
  st<-sqrt(pow(sm,2)+pow(se,2))

  C <- 1000

  for( i in 1 : N ) {
    zeros[i] <- 0
    L[i] <- pow(exp(-0.5*pow((log(x[i,2]/x[i,1])-
bt)/st,2))/(sqrt(2*3.141592654)*st)/(x[i,2]/x[i,1]),x[i,3])
    ghr[i] <- ( -1 ) * log(L[i]) + C
    zeros[i] ~ dpois(ghr[i])
  }

  fm~dlnorm(bm,taum)

  logfm<-log(fm)
  for( j in 1 : 8 ){
yy[j]<-xx[j]*fm

P2.6[j]<-1-phi((log(2.6)-bm-log(xx[j]))/sm)
P4[j]<-1-phi((log(4)-bm-log(xx[j]))/sm)
}
}
```

Representative Temperature Rise model:

```
model
{
  for ( i in 1 : N ) {
    Y[i] ~ dnorm(mu[i],tau)
    mu[i]<- (B/25)*pow(x[i],(2*0.5)-1)
  }
  tau~dgamma(0.001,0.001)
  B~dunif(0,1500)
}
```

Representative Velocity model:

```
model
{
  for ( i in 1 : N ) {
    Y[i] ~ dnorm(mu[i],tau)
    mu[i]<- A*pow(x[i],-0.333)
  }
  tau~dgamma(0.001,0.001)
  A~dunif(-15,15)
}
```

MATLAB Scripts for estimation of plume mass flow following steps outlaid in reference [37]

Main script:

```
clear all
```

```
load data_temp_flame.mat
```

```
load data_vel_flame.mat
```

```
z=0.320624405;
```

```
n=0.5;
```

```
%14.4,z(Q), 0.05812661 , 0.087189914 , 0.116253219 , 0.145316524 ,  
%0.174379829 , 0.203443134
```

```
%load data_temp_interm.mat
```

```
%load data_vel_interm.mat
```

```
%z=0.650635109;
```

```
%n=0;
```

```
%load data_temp_plume.mat
```

```
%load data_vel_plume.mat
```

```
%z=1.012384727;
```

```
%n=-.333;
```

```
%Q=14.4;
```

```
%Q=21.7;
```

```
Q=33;
```

```
%Q=44.9;
```

```
%Q=57.5;
```

```
T0=273+25;
```

```
nsample=100;
```

```
lamda=0.862;
```

```
C_B=0.9;
```

```
rho=1.2;
```

```
a=faz(z/Q^(.4),T0,data_temp,n,nsample);
```

```
% a_half=faz(z/Q^(.4),T0,data_temp,nsample);
```

```
a_half=1.0597;
```

```
UQ=fUQ(z/Q^(.4),data_vel,n,nsample);
```

```
U=UQ.*(Q^.2);
```

```

for i=1:nsample
    I(i)=fintI(lamda,a(i));
    K(i)=fintK(lamda,a(i));

    %C_lamda=sqrt((1-.26)*Q / ( pi *1 *rho*T0*U(i)*(1-
I(i))))/fsig(a(i),U(i),a_half,lamda,1,C_B,n);

    %C_lamda=.173 %Constant used to check against paper/equation: fail
    %C_lamda=sqrt(((1-.26)*2.981486877^-1) / ( pi *1
*rho*T0*a_half)/(1+a_half)))*(zQ/0.19)^((1/(4*C_B^2))-n)*sqrt(log(1+a(i))/log(1+a_half));
    %(The above equation is for the flame region only and Q of 14.4)

    %sig(i)=fsig(a(i),U(i),a_half,lamda,C_lamda,C_B,n);

    %sig(i)=fsig(a(i),lamda,C_lamda,C_B,z);
    %(The above equation is for the flame region only, equation 8b)
    sig(i)=fsig(rho,T0,a_half,z,Q,C_B,n,a(i));
    %(The above equation is for the flame region only, equation 16)
    % a_half is aF in the McCaffrey paper

    m(i)=pi*rho*(sig(i)^2)*U(i)*I(i);

end

hist(m)
title('Hist of m')

%function sig=fsig(a,U,a_half,lamda,C_lamda,C_B,n)
%J=fintJ(lamda,a,a_half,n);
%K=fintK(lamda,a);

%sig= (C_lamda*J^((lamda^2)/(4*C_B^2))) / (U*sqrt(K));

%end

Sigma:

%function sig=fsig(a,lamda,C_lamda,C_B,z)
%K=fintK(lamda,a);

%sig= C_lamda*exp((((lamda^2)/(4*C_B^2))*(log(1+a)/(a*K)))-0.5)*log(z));
%C_lamda*exp((((lamda^2)/(4*(C_B^2)))*(log(1+a)/(a*K)))-0.5)*log(z));

```



```

%end
%(The above function is for use in the flame region only)

function sig=fsig(rho,T0,a_half,z,Q,C_B,n,a)

sig= (sqrt(((1-0.26)*(3.058940993^-
1))/((pi*1*rho*T0*a_half)/(1+a_half))))*((z/Q^0.4)/(0.2))^(1/(4*C_B^2))-
n)*sqrt((log(1+a))/(log(1+a_half))))*Q^0.4;
%sig= (sqrt(((1-.26)*(3.05894^-1)) /
( (2988.33)/(1+a_half))))*((z/(Q^.4))/0.2)^(1/(4*C_B^2))-
n)*sqrt(log(1+a)/log(1+a_half))))*Q^0.4;
end
%(The above function is for use in the flame region only)

```

a:

```

function az=faz(zQ,T0,data_Bn,n,nsample)

ind=floor(1 + (20000-1).*rand(nsample,1));

B=data_Bn(ind,1);
% n=data_Bn(ind,2);

az=(B/T0).*(zQ).^2*n-1);

end

```

U:

```

function UQ=fUQ(zQ,data_vel,n,nsample)

ind=floor(1 + (20000-1).*rand(nsample,1));

A=data_vel(ind,1);
%n=data_vel(ind,2);

UQ=A.*(zQ).^n;

end

```

I:

```
function I=fintI(lamda,a)

fI=@(p)1./(1+a*p.^(1/lamda^2));
I=quad(fI,0,1);

end
```

J:

```
function J=fintJ(lamda,a,a_half,n)

K=fintK(lamda,a);

ftemp=@(p)log(1+p)./((p.^2).*K);

J=exp((1/(1-2*n))*quad(ftemp,a,a_half));

end
```

K:

```
function K=fintK(lamda,a)

fK=@(p)p./(1+a*p.^(1/lamda^2));
K=quad(fK,0,1);

end
```

Plume mass flow Output updating model:

```
+model;
{
  bm~dunif(-5,5)
  sm~dunif(0,5)
  taum<-1/pow(sm,2)
  pe<-0.15

  be<-(log(1+pe)+log(1-pe))/2
  se<-(log(1+pe)-log(1-pe))/(2*1.95996398454005)

  bt<-bm-be
  st<-sqrt(pow(sm,2)+pow(se,2))

  C <- 1000

  for( i in 1 : N ) {
    zeros[i] <- 0
    L[i] <- pow(exp(-0.5*pow((log(x[i,2]/x[i,1])-
bt)/st,2))/(sqrt(2*3.141592654)*st)/(x[i,2]/x[i,1]),x[i,3])
    ghr[i] <- ( -1 ) * log(L[i]) + C
    zeros[i] ~ dpois(ghr[i])
  }

  fm~dlnorm(bm,taum)

  logfm<-log(fm)
  for( j in 1 : 11 ){
yy[j]<-xx[j]*fm

P2.6[j]<-1-phi((log(2.6)-bm-log(xx[j]))/sm)
P4[j]<-1-phi((log(4)-bm-log(xx[j]))/sm)
}
}
```

MATLAB Code used in place of modified CFAST FORTRAN code to estimate plume mass flow:

```
function victor2(file) %Defines the function
```

```
data = xlsread('data15.xls'); %You need to change this to the importdata function  
n = 93;
```

```
for i= 1:n
```

```
    Z = data(i,1);
```

```
    Q = data(i,2);
```

```
    QJL = Q/1000;
```

```
    QC = QJL * 0.7;
```

```
    B = Z/(QC^0.4);
```

```
    for j = 1:n
```

```
        A1 = data(j,3);
```

```
        F = data(j,4);
```

```
        L = data(j,5);
```

```
        M = data(j,6);
```

```
        A2 = data(j,7);
```

```
        A3 = data(j,8);
```

```
        MLR = QJL/50000;
```

```
        if B > 0.2
```

```
            MFP(i,j) = A3*(B^M)*QC;
```

```
        elseif B > 0.08
```

```
            MFP(i,j) = A2*(B^L)*QC;
```

```
        else
```

```
            MFP(i,j)= A1*(B^F)*QC;
```

```
        end
```

```
    end
```

```
end
```

```
ME = MFP-MLR;
```

```
xlswrite('MEI15.xls',ME);
```

```
xlswrite('MFPI15.xls',MFP);
```

Bibliography

1. "10 CFR 50.48: Fire protection." Text from: *Code of Federal Regulations*. Available from: NRC.gov; Accessed 10/17/09.
2. National Fire Protection Association. *NFPA 805*: "Performance-Based Standard for Fire Protection for Light Water Reactor Electric Generating Plants. 2001 Edition," 2001
3. U.S. Nuclear Regulatory Commission, Electric Power Research Institute, "Verification and Validation of selected Fire Models for Nuclear Power Plant Applications, Volume 1 to 7," U.S. Rockville, MD, Palo Alto, CA, NUREG-1824 and EPRI 1011999, 2007.
4. M. Azarkhail, V. Ontiveros, M. Modarres. "A Bayesian Framework for Model Uncertainty Consideration in Fire Simulation Codes." 17th International Conference on Nuclear Engineering, Brussels, 2009.
5. W.W. Jones, R.D. Peacock, G.P. Forney, and P.A. Reneke, "Consolidated Model of Fire Growth and Smoke Transport (Version 6): Technical Reference Guide," NIST SP 1026, National Institute of Standards and Technology, Gaithersburg, MD, 2005.
6. E. L. Droguett. "Methodology for the Treatment of Model Uncertainty." Ph.D Thesis; University of Maryland-College Park, 1999
7. C.H. Shirazi. "Data-Informed Calibration and Aggregation of Expert Judgment in a Bayesian Framework." Ph.D Thesis; University of Maryland-College Park, 2009
8. M. Pourgol-Mohamad. "Integrated Methodology for Thermal-Hydraulics Uncertainty Analysis (IMTHUA)," Ph.D Thesis; University of Maryland-College Park, 2007

9. Technical Program Group, "Quantifying reactor safety margins: application of CSAU to a LBLOCA," NUREG: CR-5249, EG&G, Idaho, 1989
10. Technical Program Group, "Quantifying reactor safety margins: application of CSAU to LBLOCA." Nucl Eng. Des. 119, 1-117, 1990
11. R.A. Shaw, T.K. Larson, R.K. Dimenna, "Development of phenomena identification and ranking table (PIRT) for thermal-hydraulics phenomena during a PWR LBLOCA," NUREG:CR-5074, EG&G, Idaho, 1988
12. G.E. Wilson and B.E. Boyack, "The role of the PIRT process in experiments, code development and code applications associated with reactor safety analysis." Nucl. Eng. Des. 186, 23-37. 1998
13. T. Saaty. "Decision-Making for Leaders." Belmont, CA. Lifetime Learning Publications, Wadsworth Inc. 1982
14. U.S. Nuclear Regulatory Commission, Sandia National Laboratories, "A Phenomena Identification and Ranking Table (PIRT) Exercise for Nuclear Power Plant Fire Modeling Application," U.S. Rockville, MD, Albuquerque, NM, NUREG/CR-6978 and SAND2008-3997P, 2008.
15. MRC Biostatistics Unit, "*The WinBUGS Project*," Cambridge, UK.
16. M. Azarkhail and M. Modarres, "A Novel Bayesian Framework for Uncertainty Management in Physics-Based Reliability Models", ASME International Mechanical Engineering Congress and Exposition, November 11-15, Seattle, Washington, USA., 2007
17. M. K. Cowles, "Review of WinBUGS 1.4", The American Statistician, Vol. 58(4):330-336, 2004

18. R. A. Fisher, "On an Absolute Criterion for Fitting Frequency Curves", Messenger of Mathematics, Vol. 41, pp. 155-160. [Reprinted in Statistical Science, Vol. 12:39-41, 1997
19. S.S. Wilks. "Determination of sample sizes for setting tolerance limits" Ann Math Stat;12:91-6, 1941
20. S.S. Wilks. "Statistical prediction with special reference to the problem of tolerance limits." Ann Math Stat,13:400-409, 1942
21. A. Wald. "An extension of Wilks method for setting tolerance limits", Ann Math Stat 14(1):45-55, 1943
22. A. Wald., "Tolerance Limits for a Normal Distribution", The Annals of Mathematical Statistics, 17(2):208-215, 1946
23. A. Wald., "Setting of Tolerance Limits When the Sample is Large", Annals of Mathematical Statistics, 13 (4):389-399, 1946
24. A. Guba, M. Makai, L. Pal., "Statistical aspects of best estimate method-1" Reliability Engineering and Safety Systems, 80:217-32, 2003.
25. G.B. Wallis., "Contribution to the paper Statistical aspects of best estimate method-1 by Attila Guba, Makai M., Pa'l L", Reliability Engineering and System Safety 80309-11, 2003
26. L. Pal, M. Makai, "Remarks on statistical aspects of safety analysis of complex systems". arXiv:physics/0308086, 2004
27. L. Pal, M. Makai, "Statistical Considerations of safety analysis". arXiv:physics/0511140 v1, 2005

28. G. Heskestad., "Fire Plumes, Flame Height and Air Entrainment" in the SFPE Handbook of Fire Protection Engineering, 3rd Ed., National Fire Protection Association. 2002
29. G. Heskestad., "Peak Gas Velocities and Flame Heights of Buoyancy-Controlled Turbulent Diffusion Flames" Eighteenth Symposium (International) on Combustion" The Combustion Institute, Pittsburg, 1981, p. 951.
30. F.P. Ricou, and D.B. Spalding. Journal of Fluid Mechanics. 11, 21 1961.
31. G. Heskestad. "Luminous Heights of Turbulent Diffusion Flames. Fire Safety Journal, 5:103, 1983.
32. J. Gott, et al, "Analysis of High Bay Hangar Facilities for Fire Detector Sensitivity and Placement," National Institute of Standards and Technology, Gaithersburg, Maryland, USA, 1997.
33. Hostikka, S., Kokkala, M., and Vaari, J., "Experimental Study of the Localized Room Fires", VTT Technical Research Centre of Finland. 2001
34. A. Hamins, A. Maranghides, E. Johnsson, M. Donnelly, J. Yang, G. Mullholland, and R. Anleitner, "Report of the Experimental Results for the International Fire Model Benchmarking and Validation Exercise #3", NIST Special Publication 1013-1, National Institute of Standards and technology, Gaithersburg, MD, 2005.
35. "Air Properties" The Engineering ToolBox. http://www.engineeringtoolbox.com/air-properties-d_156.html
36. Wikipedia contributors. "Earth's gravity." Wikipedia, The Free Encyclopedia. Wikipedia, The Free Encyclopedia, 10 Mar. 2010. Web. 16 Mar. 2010.

37. S. De Wit, *Uncertainty in Predictions of Thermal Comfort in Buildings*, Doctoral Dissertation, Delft University of Technology, Delft, Netherlands, June 2001.
38. B.J. McCaffrey, "Momentum Implications for Buoyant Diffusion Flames", *Combustion and Flame*. 52 : 149-167, 1983.
39. B.M Cetegen, E.E. Zukouski, T. Kubota., "Entrainment and Flame Geometry of Fire Plumes", NBS-GCR-82-402, National Bureau of Standards, Gaithersburg MD, 1982.
40. E.E. Zukoski, "Properties of fire plumes," in *Combustion Fundamentals of Fire* (ed. G. Cox), Academic Press, London, 1995
41. B.J. McCaffrey, "Purely Buoyant Diffusion Flames : Some Experimental Results", NBSIR 79-1910, National Bureau of Standards, Gaithersburg, MD, 1979.
42. C.W. Spicer, M.W. Holdren, T.F. Lyon, R.M. Riggin, "Composition and Photochemical Reactivity of Turbine Engine Exhaust" Battelle Columbus Laboratories, Columbus, OH, 1984.
43. R.S. Barlow, G.J. Fiechtner, C.D. Carter, and J.Y. Chen, "Experiments on the scalar structure of turbulent CO/H₂/N₂ jet flames" *Combustion and Flame*, 120(4):549-569, 2000.
44. J. Milke, *Model 2: Analysis of Smoke Hazards, Smoke Management ENFP 629*. University of Maryland, College Park. 2009.
45. *Fire Growth and Smoke Transport Modeling with CFAST*. National Institute of Standards and Technology. <http://cfast.nist.gov/>.